

# Commercialization of Bit-Patterned Media

by

Ria Esterina

S.Si. Physics

Universitas Pelita Harapan, 2007

SUBMITTED TO THE DEPARTMENT OF MATERIALS SCIENCE  
AND ENGINEERING IN PARTIAL FULFILLMENT OF THE REQUIREMENTS FOR  
THE DEGREE OF

MASTER OF ENGINEERING IN MATERIALS SCIENCE  
AND ENGINEERING

AT THE

MASSACHUSETTS INSTITUTE OF TECHNOLOGY

SEPTEMBER 2009

©2009 Massachusetts Institute of Technology. All rights reserved.

Signature of Author: \_\_\_\_\_

Department of Materials Science and Engineering  
August 14<sup>th</sup>, 2009

Certified by: \_\_\_\_\_

Caroline A. Ross  
Toyota Professor of Materials Science and Engineering  
Thesis Supervisor

Certified by: \_\_\_\_\_

Adekunle O. Adeyeye  
Associate Professor of Electrical and Computer Engineering, NUS, Singapore  
Thesis Supervisor

Accepted by: \_\_\_\_\_

Christine Ortiz  
Associate Professor of Materials Science and Engineering  
Chair, Departmental Committee on Graduate Students



# COMMERCIALIZATION OF BIT-PATTERNED MEDIA

by

**Ria Esterina**

Submitted to the Department of Materials Science and Engineering  
on August 14<sup>th</sup>, 2009 in partial fulfillment of the requirements for the Degree of  
Master of Engineering in Materials Science and Engineering

## **ABSTRACT**

Realm of data storage density has expanded from gigabyte- to terabyte-domain. In such a high areal density, bit-patterned media is a promising candidate to overcome the superparamagnetic limit faced by the conventional continuous media. However, the patterned media concept has not been realized in mass production due to several reasons. Beside the stringent requirement of high-resolution lithography, high production cost is inevitably the major challenging problem. If a low-cost mass fabrication scheme is available, bit-patterned media will be an innovative way in hard disk technology to achieve a storage density beyond 1 Tb/in<sup>2</sup>.

The objective of this thesis is to review the patterned media technology and discuss its challenges and commercialization viability. A possible mass-production scheme is discussed. Electron beam lithography and self assembly process of block copolymer are used to fabricate the master template. To ensure high throughput, template replication as well as disk fabrication are carried out by UV-nanoimprint lithography (UV-NIL).

Considering the large opportunity of patterned media to enter the market, a business plan was constructed. Enormous profit was proved to be possible when the barrier of technology, intellectual property, and funding can be surpassed. Therefore, patterned media shows to be superior in terms of performance and cost compared to the conventional media.

Thesis supervisor: Caroline A. Ross  
Title: Toyota Professor of Materials Science and Engineering

Thesis Supervisor: Adekunle O. Adeyeye  
Title: Associate Professor of Electrical & Computer Engineering, NUS

## **Acknowledgements**

There are a lot of people who have made it possible for me to complete this thesis. First, I would like to thank Prof. Caroline A. Ross for her guidance and advice. Thank you for making this project to be a pleasurable learning experience. I am also deeply indebted to Prof. Adekunle Adeyeye from NUS, Singapore, who has always been encouraging. His advice and critiques have shaped the direction and vision of my thesis. I have also received helpful comments from Prof. Eugene Fitzgerald and Dr. Andreas Wankerl for the technology evaluation aspects.

Next, I would like to express my appreciation to Yudi for helpful discussion in developing the business plan. Thanks also to Iongying for introducing me with Zotero software and to Rhea for helping me print the draft.

Lastly, for my parents and sister in Bali, thank you for your love, support, and faith in me. Without their support, I would never have achieved what I intended to in life.

## Table of Contents

<b>Abstract</b> .....	<b>3</b>
<b>Acknowledgements</b> .....	<b>4</b>
<b>Table of Contents</b> .....	<b>5</b>
<b>List of Figures</b> .....	<b>7</b>
<b>List of Tables</b> .....	<b>10</b>
<b>Chapter 1 Introduction</b> .....	<b>11</b>
<b>Chapter 2 Bit-Patterned Media Technology</b> .....	<b>13</b>
2.1. Fundamentals of Magnetic Recordings .....	<b>13</b>
2.2. Limitations of Conventional Perpendicular Media .....	<b>15</b>
2.3. Prospects of Bit-Patterned Media .....	<b>17</b>
2.4. Challenges to Bit-Patterned Media Technology .....	<b>18</b>
2.4.1. Media Fabrication .....	<b>18</b>
2.4.2. Magnetic Properties Uniformity .....	<b>20</b>
<b>Chapter 3 Fabrication of Bit-Patterned Media</b> .....	<b>27</b>
3.1. Structures of Recording Media .....	<b>27</b>
3.2. Template Fabrication .....	<b>29</b>
3.3. Media Fabrication .....	<b>35</b>
<b>Chapter 4 Market Opportunity</b> .....	<b>40</b>
4.1 Technology Supply Chain .....	<b>40</b>
4.2 Competing Technologies .....	<b>41</b>
4.2.1. Heat-Assisted Magnetic Recording .....	<b>41</b>
4.2.2 Microwave-Assisted Magnetic Recording .....	<b>43</b>
4.2.3. Exchange Coupled Composite Media .....	<b>45</b>
4.2.4. Comparison among HAMR, MAMR, and ECC media .....	<b>46</b>
4.2.5. Outer Competitor .....	<b>47</b>
4.3. Complementary Technologies .....	<b>48</b>
4.3.1 Head Technology .....	<b>48</b>
4.3.2. Disk Drive Electronics .....	<b>53</b>
4.4. Intellectual Property .....	<b>54</b>

4.5. Target World Market .....	57
<b>Chapter 5 Business Plan .....</b>	<b>60</b>
5.1 Operational Plan .....	60
5.2 Capitalization .....	63
5.3 Financial Plan .....	64
<b>Chapter 6 Conclusion .....</b>	<b>73</b>
<b>References.....</b>	<b>75</b>
<b>Appendix 1: Block Copolymers on Chemically Heterogeneous Striped Surface ....</b>	<b>80</b>
<b>Appendix 2: NIL Cost Calculation .....</b>	<b>83</b>
<b>Appendix 3: Ion Miller Throughput Calculation .....</b>	<b>84</b>
<b>Appendix 4: Sputtering and Dry Etching Machine Throughput Calculation .....</b>	<b>85</b>
<b>Appendix 5: EBL Cost Calculation .....</b>	<b>87</b>

## List of Figures

Fig. 1.1. Areal density trend .....	11
Fig. 2.1. Hysteresis loop of a permanent magnet .....	13
Fig. 2.2. Magnetostatic and domain-wall energies versus particle size .....	14
Fig 2.3. Magnetization change of a very small particle (single-domain particle) .....	14
Fig 2.4. Hysteresis behavior of a single-domain particle with the external field applied along (a) the easy axis, and (b) the hard axis .....	15
Fig 2.5. Hysteresis behavior of superparamagnetic materials .....	16
Fig 2.6. Coercivity versus size for a small particle .....	16
Fig. 2.7. Disk coercivity versus areal density evolution .....	17
Fig. 2.8. Schematic of (a) conventional thin film medium, consisting of single-domain grains. Bits are represented as transitions between regions of opposite net magnetization. Each bit occupies an area of tens to hundreds of grains. (b) Patterned medium with in-plane magnetization. Now the bits are defined lithographically with a period $p$ . The bits can either be polycrystalline (indicated by dotted lines) or single crystal, but they magnetically act as single domains. (c) Patterned medium with out-of-plane magnetization. The period, height, and diameter are $p$ , $h$ , and $d$ , respectively. Binary one and zero are indicated .....	18
Fig. 2.9. Coercivity distribution map of patterned media obtained by dot-by-dot analysis. The contrast indicates $H_c$ .....	21
Fig. 2.10. MFM image of patterned media written by ring head. Black lines indicate a trajectory of the ring head .....	21
Fig. 3.1. Proposed fabrication plan of BPM .....	27
Fig. 3.2. Functional layers of perpendicular recording medium. Layers are not to scale .....	28
Fig. 3.3. Chemically-assisted pattern generation .....	30
Fig. 3.4. SEM images of lamellae-forming PS- <i>b</i> -PMMA block copolymer films ( $L_0 = 48$ nm) on chemically nanopatterned substrates as a function of $L_S$ ( $L_S = 42.5$ nm, 47.5 nm, and 52.5 nm) and composition of the random-copolymer brush used to create the chemical pattern. The blue beads represent PS units and red beads represent PMMA units in the random block copolymer brush layer. Higher percentages of PS in the random block copolymer brush produce the higher chemical contrast of the surface patterns to PS- <i>b</i> -PMMA. Stronger chemical contrast favors replication of the underlying pattern .....	31
Fig. 3.5. Process to create lithographically defined, chemically pre-patterned surfaces, and subsequent directed assembly. (A) Electron-beam lithography patterns at $L_S = L_0$ (left) and $L_S = 2L_0$ (right). (B) Chemical contrast on the substrate after $O_2$ plasma	

exposure on the e-beam–defined spots above. (C) Block copolymer thin film. (D) Guided self-assembly in registration with the underlying chemical pattern .....	32
Fig. 3.6. Rotary-stage EBL .....	32
Fig. 3.7. Servo pattern element write using the CSFL function. (a) Groove and dot, (b) dot and shifted elliptical dot, (c) groove and right-angled groove, and (d) different-length pits with various doses .....	33
Fig. 3.8. Self-assembly of block-copolymer .....	35
Fig. 3.9. UV-NIL process for patterned media .....	36
Fig. 3.10. Patterned media imprint examples .....	36
Fig. 3.11. Steps in the fabrication of patterned magnetic media .....	37
Fig. 3.12. Magnetic spacing requirements for HDD .....	38
Fig. 3.13. Illustration of high throughput disk fabrication with the proposed fabrication plan .....	39
Fig. 4.1. HDD supply chain .....	40
Fig. 4.2. Globalization of HDD supply chain .....	41
Fig.4.3. Diagram of HAMR writing process .....	42
Fig. 4.4. MAMR process .....	43
Fig. 4.5. (a) Schematic illustration of the $ac$ field assisted perpendicular head design. (b) Illustration of magnetization precession of the field generating layer facilitated by the spin torque. $\sigma_{int}$ is the interlayer exchange coupling surface energy density, $M_S$ is the saturation magnetization, and $\delta$ is the thickness .....	44
Fig. 4.6. Illustration of a grain in an ECC medium. It consists of a magnetically hard part and a magnetically soft part .....	45
Fig. 4.7. Basic structure of proposed ECC media .....	46
Fig. 4.8. Comparison between HDD and SSD .....	47
Fig. 4.9. (a) Evolution of head technology; (b) Structure of CPP TMR and CPP GMR heads .....	49
Fig.4.10. Trends of data transfer rate for high-end HDD systems and allowed resistance-area product ( $RA$ ) of read head sensors with CPP structure versus areal density .....	50
Fig 4.11. Estimated required $\Delta RA$ of CPP-GMR for higher recording densities for output signal voltage = 1.5 mV, head efficiency = 30%, sense current density = 100 MA/cm <sup>2</sup> , power consumption of sensor element = 0.6 mW .....	51
Fig. 4.12 Standard feedback block diagram .....	54
Fig. 4.13. Trend in HDD application .....	57



Fig. 4.14. HDD shipments and revenue .....	<b>58</b>
Fig. 4.15. HDD industry forecast and market share .....	<b>58</b>
Fig. 4.16. Worldwide PC shipments forecast .....	<b>59</b>
Fig. 5.1. Diagram plots of the price-per-GB for NAND Flash memory and HDDs. As of Mar 2009, NAND Flash memory is about US\$1.25 per GB. Prices through Mar 2009 from <i>Nihon Keizei Shimbun</i> , beyond that forecasts by <i>Nikkei Electronics</i> .....	<b>65</b>
Fig. 5.2. Cost/GB for 1Tb/in <sup>2</sup> as a function of production volume .....	<b>67</b>
Fig. 5.3. Cost/GB as a function of production volume and areal density .....	<b>67</b>
Fig. 5.4. Maximum cost per disk and cost per GB for different areal densities .....	<b>69</b>
Fig. 5.5. Contour representation of cost/GB as a function of production volume and areal density .....	<b>69</b>
Fig. 5.6. Annual profit projection of HDD media company with BPM technology .....	<b>71</b>
Fig. 5.7. Profit margin projection of HDD media company with BPM technology .....	<b>72</b>
Fig. A1.1. When the width of the stripes is much larger than the size of a block, the copolymers may either form 3D brushes within each stripe ( <i>a</i> ) or 2D brushes along the interfaces between the stripes ( <i>b</i> ) .....	<b>80</b>
Fig. A2.1. Imprio <sup>®</sup> HD2200 .....	<b>83</b>
Fig. A3.1. FAB104 ion miller system .....	<b>84</b>
Fig. A4.1. PT770 Dry Etcher system .....	<b>85</b>
Fig. A5.1. JBX-9300FS EBL system .....	<b>87</b>

## List of Tables

Table 2.1. Examples of required lithography dimensions for patterned media .....	19
Table 4.1. Read head challenges .....	48
Table 4.2. Geometrical requirements for head for patterned media .....	48
Table. 4.3. Various design scenarios for BPM recording systems .....	52
Table 4.4. Several relevant patents to BPM .....	55
Table 5.1. Comparison of start-up company formats .....	60
Table 5.2. Additional cost breakdown for PV = 100 M disks/year and Capacity = 600 GB/disk .....	62
Table 5.3. Start-up capital calculation for PV = 100M disks/year .....	63
Table 5.4. Cost modeling for 100M disk/year throughput .....	66

## 1. Introduction

Hard Disk Drive (HDD) is a robust industry with shipments of 593.2 million units in 2008, up by 14.93 percent compared with 516.2 million units in 2007, according to a market research firm iSuppli Corp. [1]. The history of magnetic recording technology dates back to 1898 when Valdemar Poulsen patented the telegraphone [2]. Its application to HDD industry began in 1956 when IBM introduced Random Access Method of Accounting and Control (RAMAC) with an areal density of approximately 2 kb/in<sup>2</sup> [3]. Since then, the areal density of HDD has been improved to meet the ever-increasing requirement of performance. As shown in Fig. 1.1, there has been more than a three-order-of-magnitude increase of areal density since 1990s, suggesting that HDD industry is on the way to enter the terabyte-era. To ensure a smooth transition, there is a strong driving force for HDD industry to shift from the conventional continuous-grain magnetic media to bit-patterned media (BPM).

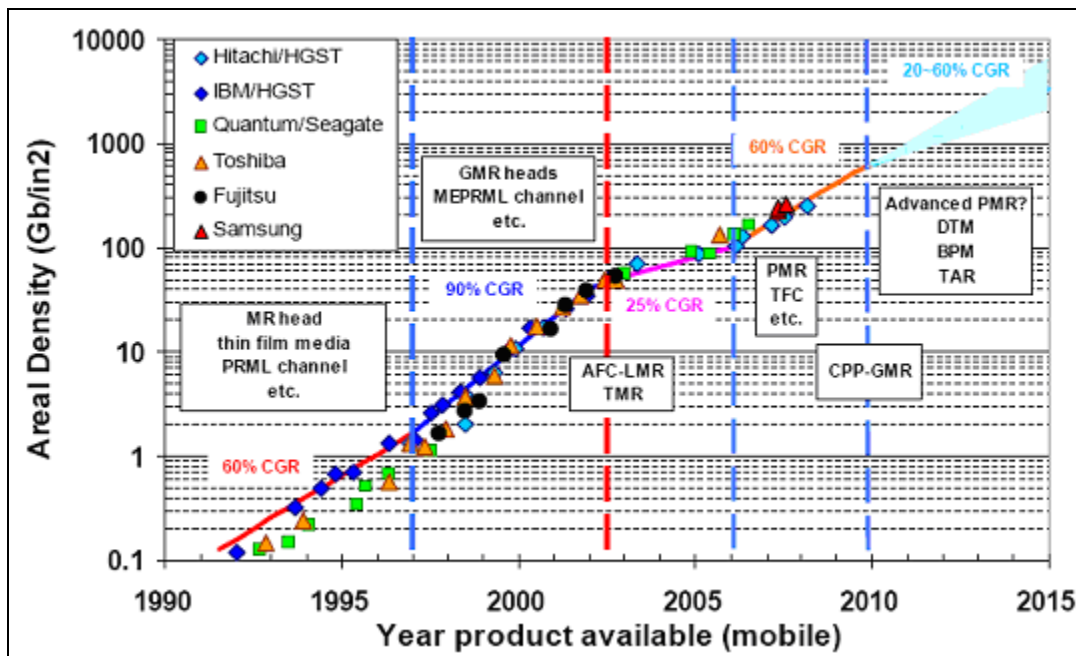


Fig. 1.1. Areal density trend [4].

Conventional HDD records data by writing the magnetization pattern on a thin film with perpendicular magnetic anisotropy axis. However, terabyte storage density is not a possible scheme with this current conventional method. In continuous thin film media,

one bit consists of several grains or magnetic units. As the density of data storage increases, superparamagnetic phenomenon occurs. Magnetic recording trilemma, among SNR, areal density, and thermal stability, is inevitable. Consequently, perpendicular magnetic recording (PMR) technology is predicted to reach its limit at 600 Gb/in<sup>2</sup> [5]. BPM, firstly proposed in 1989 by Nakatani et al. [6], is a promising candidate to surpass this limitation. BPM stores the data on a uniform array of magnetic cells, each of which will store one bit of information. In contrast with PMR, the bits in BPM, either polycrystalline or single crystal, act as single-domain magnets. The data density of BPM could extend to 1000 times that of continuous media [7].

Nonetheless, the commercialization of BPM is faced with several challenges. Despite the fact that patterned media concept has been reported since 20 years ago, it has not been realized in mass production. There had been various proposals of possible mass-production schemes until 2008 when two major data storage companies, Hitachi and Seagate, shared the same view on a single most optimum manufacturing strategy for BPM [8],[9]. Beside the stringent requirement of high-resolution lithography, high production cost is inevitably the major challenging problem. Not until its production cost is lower or comparable to the cost of conventional method will the commercialization of BPM be feasible.

The objective of this thesis is to review the BPM technology and discuss its commercialization viability. A brief introduction about HDD and its recording schemes is given in Chapter 1. The idea of BPM technology and its manufacturing method are detailed in Chapter 2 and 3. The market opportunity and business plan are discussed in Chapter 4 and 5, respectively. Finally, Chapter 6 concludes the thesis.

## 2. Bit-Patterned Media Technology

### 2.1. Fundamentals of Magnetic Recordings

HDD belongs to the group of magnetic storage. It integrates many key elements, one of which is the magnetic recording media. To have a clear picture of the magnetic recording media, it is essential to understand the physics behind the magnetic recording process.

Magnetic properties of a material are typically characterized by its hysteresis loop, as shown in Fig. 2.1.

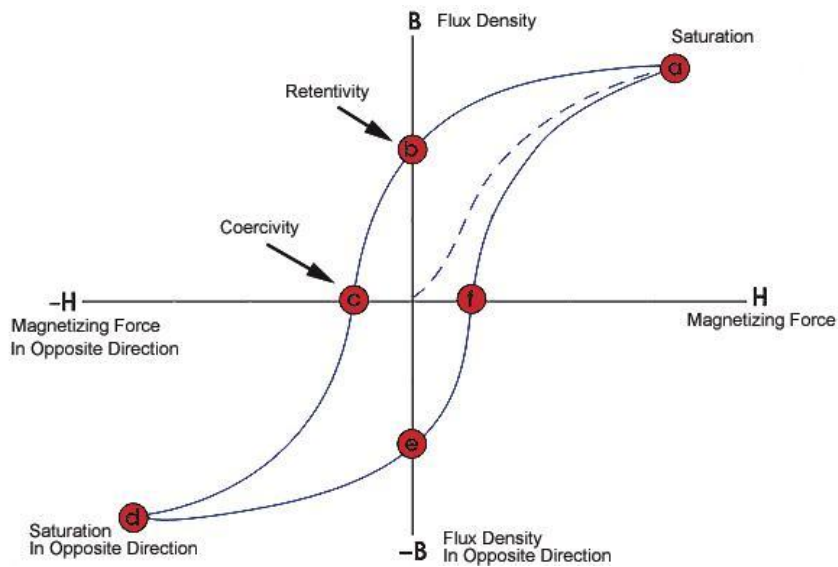


Fig. 2.1. Hysteresis loop of a permanent magnet [10].

Hysteresis is the result of an irreversible conversion from energy to heat, with the energy lost in going round a cycle is equal to the area inside the major loop. In this loop, we can observe two important properties of a permanent magnet: remanence and coercivity. Remanence is the ability of a material to retain its magnetization after the magnetic field causing the material to achieve saturation is removed, while coercivity is the amount of required reverse magnetic field to bring the magnetization back to zero [11]. It is remanence which makes the recording process possible.

A particle can have either multi domains or single domain depending on its size. Different magnetic domains on a particle will be separated by a transition zone in between which is called the domain wall. A large particle will show multi-domain

behavior while a particle less than  $1 \mu\text{m}$  long is single-domain in zero external field [11]. This phenomenon is derived from energy consideration. As can be seen in Fig. 2.2, The domain wall energy is proportional to the area of the wall ( $\sim L^2$ ) while the magnetostatic energy is proportional to the particle volume ( $\sim L^3$ ). Therefore, a large particle will arrange itself to minimize its magnetostatic energy by creating magnetic domains, and hence multi-domain configuration. Meanwhile, a smaller particle will prefer a single-domain configuration to minimize its domain wall energy.

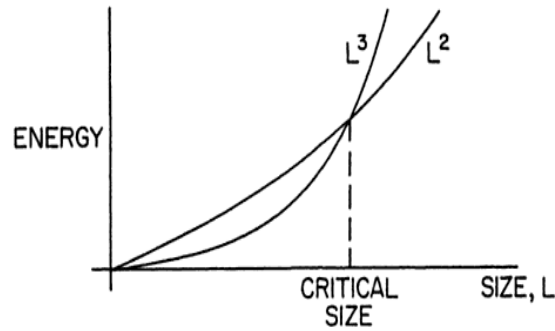


Fig. 2.2. Magnetostatic and domain-wall energies versus particle size [11].

For a small single-domain particle under an applied magnetic field, the magnetization process proceeds by rotation of the total magnetic moment of the particle, as shown in Figure 2.3. The hysteresis behavior is depicted in Figure 2.4. Due to anisotropy, a particle will have easy and hard axes. If a sufficiently large magnetic field is applied parallel to the hard direction of the particle, the M-H curve will be linear, which means there is no hysteresis. The magnetic moment will rotate towards the field direction and rotate back to its easy axis when the field is removed. On the other hand, if the field is applied along the easy axis, the magnetic moment must rotate through the hard direction to fully reverse its orientation. In this regard, the coercivity will be large, and the particle will exhibit square hysteresis loop.

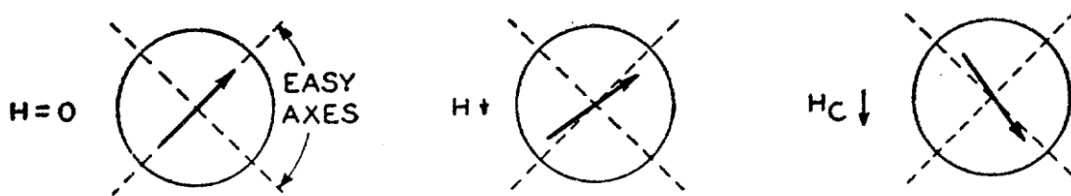


Fig 2.3. Magnetization change of a very small particle (single-domain particle) [12].

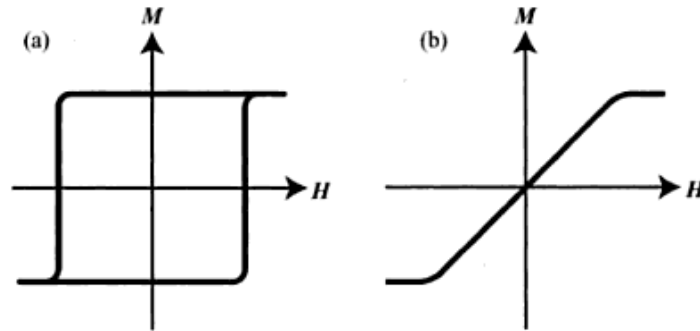


Fig 2.4. Hysteresis behavior of a single-domain particle with the external field applied along (a) the easy axis, and (b) the hard axis [13].

For magnetic recording application, it is preferable to use small single-domain particles with the writing magnetic field applied parallel to the easy axes. The recorded data is stable because a considerable force is required to switch the orientation of the magnetic moment.

## 2.2. Limitations of Conventional Perpendicular Media

In conventional perpendicular media recording (PMR), one bit consists of many grains. To achieve high areal density, the bit must be as small as possible. In this case, to ensure high signal-to-noise ratio (SNR), a large number of grains per bit cell is needed. Thus, the size of the grains must also be lowered. However, as the scaling down continues, the superparamagnetic effect is inevitable. Superparamagnetism is anhysteretic behavior of magnetization loop which is observed at temperature well above the blocking temperature (TB) [14]. Superparamagnetism is similar to paramagnetism, except that the magnetization is much larger in the former because each particle behaves like a giant spin, as depicted in Fig. 2.5.

In superparamagnetism, a particle exhibits zero coercivity and zero remanence. As we decrease the particle diameter, the coercivity will increase until the particle has reached a critical size, below which the coercivity will decrease down to zero (Fig. 2.6). This critical size depends on the particle anisotropy. Typically, for an anisotropic spherical particle at room temperature, superparamagnetism will be observed when the particle diameter is less than  $100 \text{ \AA}$  [15].

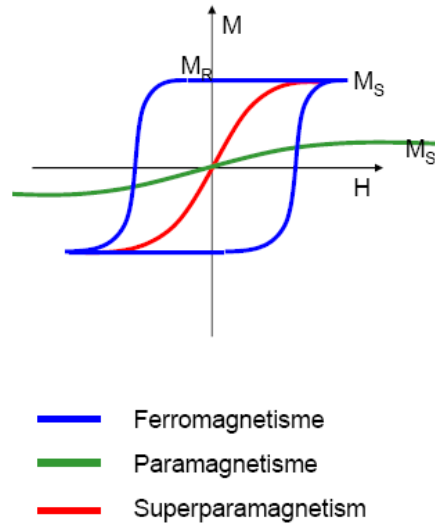


Fig 2.5. Hysteresis behavior of superparamagnetic materials [16].

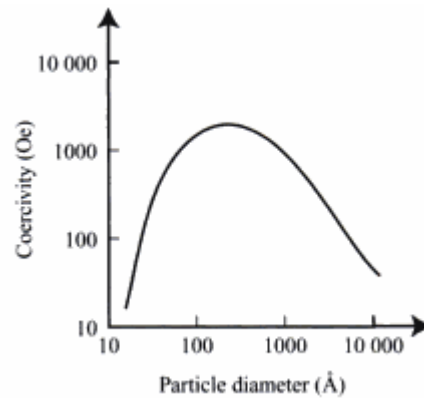


Fig 2.6. Coercivity versus size for a small particle [13].

Due to this paramagnetic effect, the small grains become magnetically unstable and tend to spontaneously flip, causing loss of data. To maintain magnetic stability for about 10 years, the ratio between magnetic energy and thermal energy of a magnetic medium should not be less than 40 ( $KV/kT \geq 40$ , where  $K$  is the anisotropy constant,  $V$  is the grain volume,  $k$  is the Boltzmann constant, and  $T$  is the temperature in Kelvin) [17]. To prevent data loss, we need to use a material with high anisotropy constant  $K$ . However, this material will then possess a very high coercivity and need a very high magnetic field to be magnetized for data recording. The coercivity evolution due to increase in areal density is shown in Fig. 2.7. The three requirements of high SNR, high areal density, and



good writability thus create a trilemma in magnetic recording. PMR scenario is thus expected to reach its limit at an areal density of  $600 \text{ Gb/in}^2$  [5].

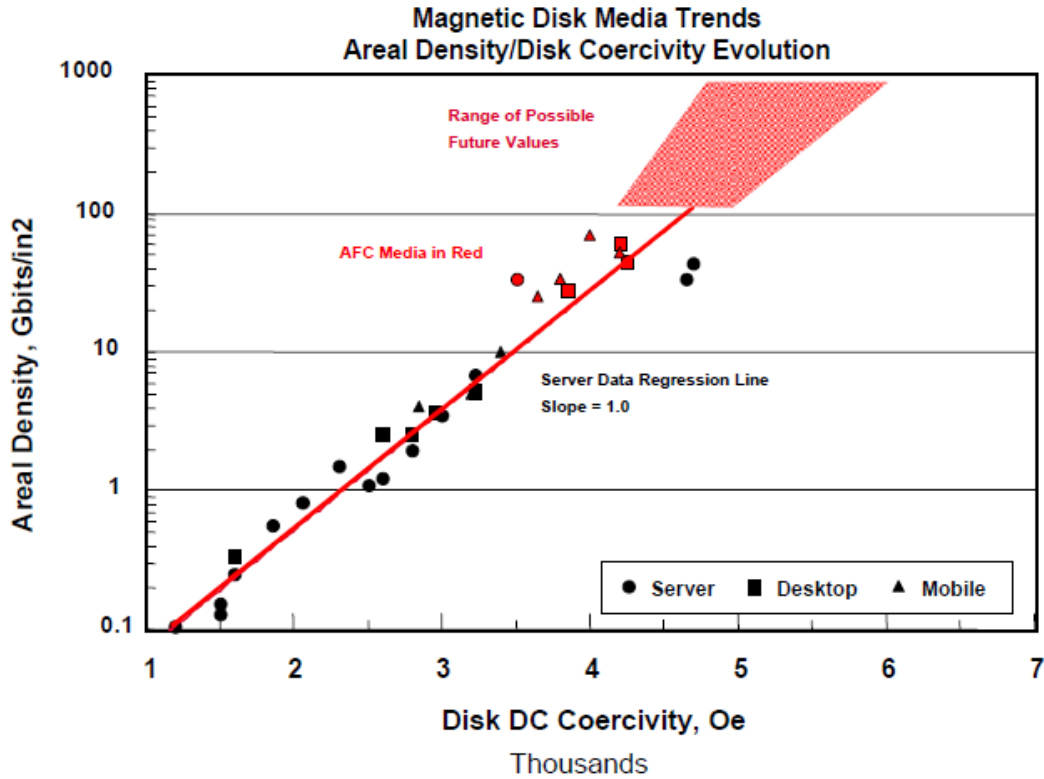


Fig. 2.7. Disk coercivity versus areal density evolution [18].

### 2.3. Prospects of Bit-Patterned Media

In BPM technology, the trilemma in magnetic recording is addressed by modifying the recording media. The media are patterned so that one bit is one magnetic entity. The restriction  $KV > 40 kT$  still holds except that  $V$  is now the bit volume, which is obviously larger than the grain volume. Thus, the thermal limit can be satisfied without sacrificing the writability. Stable high-density media can be achieved by using this technology. Areal density beyond  $1 \text{ Tb/in}^2$  is expected to be achievable in BPM. Currently, the best achievable resolution of block copolymers (BCP) is 3 nm, equivalent to approximately  $10 \text{ Tb/in}^2$  areal density [19].

Transition jitter is also eliminated in BPM since the bits are isolated one from another. Moreover, unlike the conventional media, the track width in BPM can be reduced without affecting the SNR. This can further increase the areal density of BPM [5]. To isolate the

magnetic entities, physical spacing or filling of non-magnetic materials can be used. The comparison between continuous media and BPM is shown in Fig. 2.8.

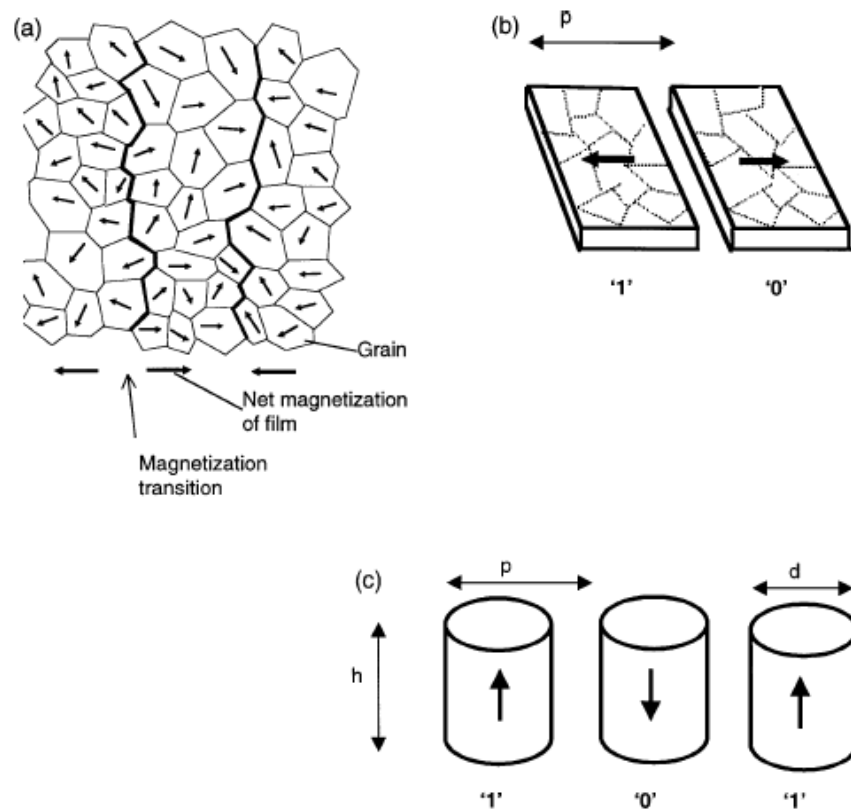


Fig. 2.8. Schematic of (a) conventional thin film medium, consisting of single-domain grains. Bits are represented as transitions between regions of opposite net magnetization. Each bit occupies an area of tens to hundreds of grains. (b) Patterned medium with in-plane magnetization. Now the bits are defined lithographically with a period  $p$ . The bits can either be polycrystalline (indicated by dotted lines) or single crystal, but they magnetically act as single domains. (c) Patterned medium with out-of-plane magnetization. The period, height, and diameter are  $p$ ,  $h$ , and  $d$ , respectively. Binary one and zero are indicated [7].

## 2.4. Challenges to Bit-Patterned Media Technology

Unfortunately, the implementation of BPM still faces several challenges associated with media fabrication and micromagnetic characteristics. Apart from those aspects, there are also challenges in the read/write head and signal synchronization as the complementary technologies, which will be addressed in Chapter 4.

### 2.4.1. Media Fabrication

The major challenge on fabricating BPM is the requirement of high resolution to lithographically pattern every bit on the disk. Examples of required lithography

dimensions for various areal density and bit aspect ratio (BAR) are given in Table 2.1. Several issues are apparent. First, because the bit locations are predefined on the disk, the head field needs to be synchronized to them. Second, to minimize disk-drive error rates, the lithography tolerance should only be a few nanometers or less. Moreover, there is a need of arranging the bits on circular tracks in order to continue using rotating disk and flying head, a need of controlling the long-range order of the pattern arrays, a need of two-sided patterning because the disk drives record on both sides of a disk, and a need of inexpensive fabrication method [20]. To be economically competitive, HDD with this BPM technology must maintain the inherent cost advantage compared to other storage technology such as semiconductor-based storage.

Table 2.1. Examples of required lithography dimensions for patterned media [20].

Density (Gb/in <sup>2</sup> )	Bit area (nm <sup>2</sup> )	Center-to-center distance (nm), along track (BAR = 1)	Center-to-center distance (nm), along track (BAR = 4)
500	1290	35.9	18
750	860	29.3	14.7
1000	625	25.4	12.7
2500	258	16.1	8
5000	129	11.4	5.7
10,000	64.5	8	4

Intermediate approaches in implementing the idea of BPM have been carried out by patterning the servo marks and patterning the individual tracks, which is termed discrete track recording (DTR) [21]. From patterning the servo marks to DTR and BPM, there are increase in areal density gain as well as the complexity and cost.

Patterning the servo marks in all the disks is a serial process, resulting in low throughput. Servo marks define the track position and thus are useful for the head to write and read the data bits reliably. Patterning the servo marks in a master and subsequently transferring the pattern to the disks by parallel process such as magnetic lithography will increase the throughput. While in DTR, the track edge noise is eliminated, leading to

improved areal density [22]. The thermal stability unit in DTR is still one grain which means that the areal density gain in DTR is lower compared to BPM.

Both servo marks patterning and DTR introduce lithography steps in their processing. The progress of DTR, especially, can be considered as a stepping stone for BPM technology although the processing requirements, in terms of resolution and tolerance, are less stringent than those in BPM.

#### **2.4.2. Magnetic Properties Uniformity**

In designing BPM, it is desirable to achieve uniform magnetic properties of the bit array. However, in practice, it is difficult to control the micromagnetic characteristics and structures.

Y. Kamata *et al.* in 2006 [23] performed a study on CoCrPt-patterned media. The CoCrPt-patterned media was fabricated by templated self-assembly of PS-PMMA and subsequent nanoimprint lithography (NIL). It is found that the mean dot volume is about  $4.2 \times 10^{-17} \text{ cm}^3$  ( $\sigma = 2.9 \times 10^{-17} \text{ cm}^3$ ). The dot height is 40 nm (original CoCrPt film thickness: 40 nm) and the mean dot diameter is about 34 nm ( $\sigma = 4.1 \text{ nm}$ ). The reasons for the dispersion of the dot diameter are the grain size and crystallinity of the CoCrPt film and the dispersion of the size of the self-assembled PS-PMMA structure used as an etching mask. Non-uniformity in the etching process may also cause dot size deviation [24]. To reduce the dispersion, optimization of the compositional ratio of PS and the PMMA polymer or choosing another self-assembling material can be done.

Similar to the continuous film, the delta-theta value from the X-ray diffraction (XRD) rocking curve analysis showed that the direction of the magnetic easy axis deviated randomly from dot-by-dot within a range of  $15^\circ$ . In this case, poor crystallinity and thick grain boundaries of a continuous film are the origin of the easy axis distribution. A patterned dot is separated into grains by grain boundaries and thus each dot has macroscopic angle dispersion as a unique property [24].



Fig. 2.9. Coercivity distribution map of patterned media obtained by dot-by-dot analysis. The contrast indicates  $H_c$  [23].

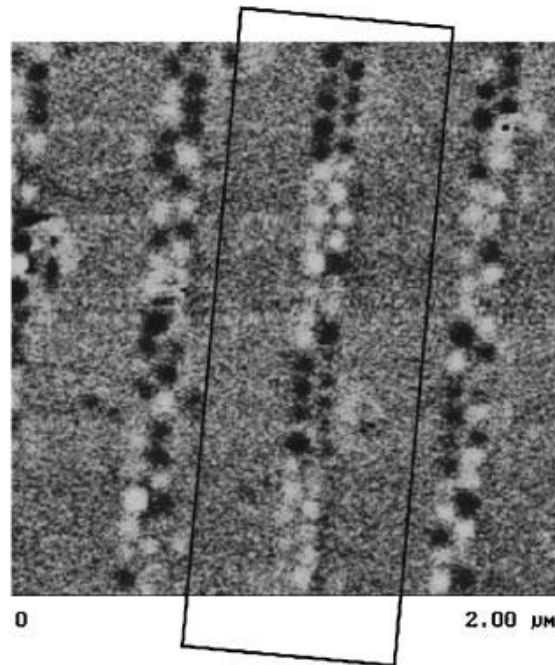


Fig. 2.10. MFM image of patterned media written by ring head. Black lines indicate a trajectory of the ring head [23].

Besides the dot size variation, magnetic particles in an array will show a distribution of switching fields, causing some particles to switch at different applied fields from others. An investigation of the microscopic deviation of magnetic properties of CoCrPt-patterned media by atomic force microscopy (AFM) and magnetic force microscopy (MFM) was also conducted by Y. Kamata et al [23]. From observation of the magnetization reversal of each dot, a few misreversed dots were clearly seen in the written “bit” patterns. The distribution of coercivity  $H_C$  was investigated by MFM using dot-by-dot analysis in the

presence of a magnetic field and the result can be seen in Fig. 2.9. It was found that  $H_C$  is about 4 kOe on the average with a wide distribution ranging from 0.5 to 7.5 kOe. This large and spatially random distribution of  $H_C$  is responsible for magnetization reversal defects as can be seen in Fig. 2.10.

Damage by the ion milling process has been said as the possible origin of the  $H_C$  deviation. But, only little change was found in the magnetic anisotropy energy from experimental and numerical estimations [24].

This spread of switching fields is attributed to small differences in shape, size, or microstructure between the particles. This will create intrinsic variability of the switching fields, which is often modeled by a Gaussian distribution [25]. A reduction in coercivity due to thermal fluctuation was expected for smaller dots. However, it was found that there is no correlation between the dot size and coercivity [23]. Microscopic intrinsic distribution of the magnetic properties and long-range magnetic dipole interaction between patterned dots are considered as the most possible origins. A continuous film sample before etching exhibits intrinsic distribution in the form of a grain-to-grain distribution as well as poor crystal orientation. When this film is processed into a patterned medium, a dot-to-dot difference in magnetic properties can be observed. To know the origin of  $H_C$  distribution, methods to estimate the distribution both in continuous film and in dot patterns are necessary [24]. The problem of  $H_C$  distribution can be resolved through the development of new magnetic materials suitable for patterning and read-write design of the patterned media [6].

Magnetostatic interactions between particles, which generate the net field acting on each particle in the array is also likely to be the cause of  $H_C$  distribution [25]. These interactions lower the energy barrier for moment flipping and therefore pose a more stringent restriction on the thermal stability. Under this consideration, a simple model is built to reproduce the hysteresis loop. In this model, the particle array is assumed to have out-of-plane magnetization and Gaussian switching fields ( $H_C$ , with standard deviation  $\sigma \ll H_C$ ). For a square array of particles, the total magnetic field acting on any particle is

equal to  $9H_i$ , where  $H_i$  is the nearest neighbor interaction field. Here, to a first approximation, magnetized elements are treated as dipoles. In this approximation,  $H_i = m/4\pi\mu_0r^3$ , where  $m$  is the moment of each particle and  $r$  is the spacing.

This interaction field  $H_i$ , acting on each particle is demagnetizing and causing a broadening of the switching field distribution. If we consider that all the particles are magnetized up and the switching field of a particle is given by  $H_{sw}$ , the particle will switch when the applied external reverse field reaches  $(H_{sw} - 9H_i)$ . In contrast, if a particle magnetized up is surrounded by particles magnetized down, an external field of  $(H_{sw} + 9H_i)$  will be needed to reverse it. It is found that without magnetostatic interactions, the collective hysteresis loop is square, while if the interactions are included, the hysteresis loop becomes sheared, with a slope proportional to the nearest neighbor interaction field ( $H_i$ ).

If the maximum interaction field is smaller than the switching field, the magnetization state is stable for any particle, independent of the magnetization direction of its neighbors. The remanence will be perfect unity. However, if the interactions are sufficiently large, which is defined as  $9H_i > H_{sw}$ , the saturated state is unstable at remanence, causing the particles to spontaneously flip their magnetization owing to interactions from their neighbors. The requirement  $9H_i < H_{sw, min}$  where  $H_{sw, min}$  is the smallest switching field of a particle in the array (which can be taken as  $H_c - 3\sigma$ ), must be fulfilled such that interaction fields alone cannot reverse the magnetization of an element.

In contrary, magnetostatic interactions for arrays with in-plane magnetization might result in better magnetic properties. In this case, if all particles are magnetized parallel to each other, the interaction fields from the neighbors can be either demagnetizing or stabilizing the magnetization. If the interactions stabilize rows of particles with aligned magnetization, the collective hysteresis loops can even be made squarer. Experiments on magnetized bars demonstrate that the switching field decreases as the lateral bar spacing is decreased [25].

In a patterned medium, the strength of interactions is determined by the proximity between the particles, but the resulting interaction will still be smaller than those in thin film media. For example, patterned media elements made of high  $K_U$  materials could remain thermally stable even in the size of a few nanometers. H.J. Richter *et al.* reported a design for recording on BPM for areal density  $1 - 5 \text{ Tb/in}^2$  with assumption that the deviation in the magnetic properties of each dot is less than 0.5% [24]. However, in practice, it is difficult to achieve such small deviation.

To eliminate the micromagnetic distribution, precise control on the lithography, assembly processes, and the microstructure of the particles, which will then improve the uniformity of the array, must be done. We can also minimize the magnetostatic interaction either by lowering the moment of the particles or increasing the spacing between them. However, reduced moment of the particles will consequently reduce their readback signal and increased spacing between the particles inevitably leads to reduced areal density [25].

From the above discussion, however, it is clear that the minimum unit of the distribution is a single magnetic grain. In BPM, a dot may be divided by grain boundaries into sub-structure. Thus, it is expected that the origin of the deviation in magnetic properties, i.e. thermal fluctuation and/or size distribution, is this sub-structure or sub-grain in each dot [24].

An obvious solution is a single-crystal dot made by a single-crystal continuous magnetic film. To achieve this, all the multiple number of underlayers, which are necessary to control the magnetic properties, should be single crystal too. We would need a single-crystal substrate which is impractical in the fabrication process.

Another alternative is a polycrystalline dot made by a polycrystalline continuous magnetic film with ultra-fine grains, about ten or more sub-grains. Sufficiently thin grain boundaries are important to reduce the size distribution of the dots. By this design, we can average out the intrinsic distribution of the magnetic properties by the strong exchange interaction between sub-grains in a dot. In this design, for the case of more than



5 Tb/in<sup>2</sup>, we need to develop nanocrystalline magnetic film as well as underlayers with grain size less than a few nm.

Amorphous dot may be an ideal design. Many kinds of amorphous magnetic film made by rare earth and transition metal alloy such as TbFeCo have been developed for application in magneto-optical recording media. Advantages of this amorphous dot is easy control of the magnetic properties by controlling the composition and perpendicular anisotropy is obtained by a sputtering deposition process without using a specific underlayer. However, several challenges also appear. Though the XRD measurement shows typical amorphous signals, microscopic columnar structure is observed. It may cause distribution in magnetic properties of the dots. Because the microscopic magnetic properties should be uniform in the range of a few nanometers, the atomic structure should also be completely random in the range of a few nanometers. Besides, the structure should be uniform in the range of inches. The sensitivity of the rare earth materials to oxygen may also cause etching damage [24]. Finally, it is difficult to tailor anisotropy in amorphous dots since they do not have magnetocrystalline anisotropy.

The necessary properties of patterned magnetic media, such as switching field, anisotropy, magnetic moment, and geometry, have not been well established for either in-plane or out-of-plane recording system. However, some general guidelines can be made. Maximizing areal density and readback signal favors a densely packed array of high-moment particles with perpendicular magnetization. However, this will create strong interactions between the particles. Meanwhile, the writing process imposes an even more stringent requirement on particle uniformity. In order to write data faithfully, the write element is required to apply a localized field to one element without writing its neighbor. If the switching fields of the neighbors vary by  $\sigma$ , the head field gradient must be much greater than  $\sigma/r$ , where  $r$  is the array period, in order to safely write one element but not its neighbor. It is found from dynamic calculations that switching appears to occur more rapidly for low-aspect ratio particles. Therefore, short particles with magnetocrystalline anisotropy are preferable over tall particles with shape anisotropy [25].

In the case of readback, it is not necessary to uniformly magnetize the elements to saturation, as long as there is sufficient remanence to be detected by the recording system. Several possible readback schemes are detecting the magnetization directly (such as a near-field magneto-optical probe), the field above the element (such as in an MR head), or the field gradient above the element (such as in MFM). Most readback methods described in the literature, however, rely on the detection of either field or field-gradient, so that the fields from neighboring particles will affect the readback and could introduce signal jitter.

### 3. Fabrication of Bit-Patterned Media

In 2008, Hitachi and Seagate proposed a common fabrication plan, which can be seen in Fig. 3.1. The plan, which promisingly enables high resolution and high throughput, inserts some new steps into the traditional PMR disk process flow. The fabrication plan can be divided into two main processes, template fabrication and media fabrication process.

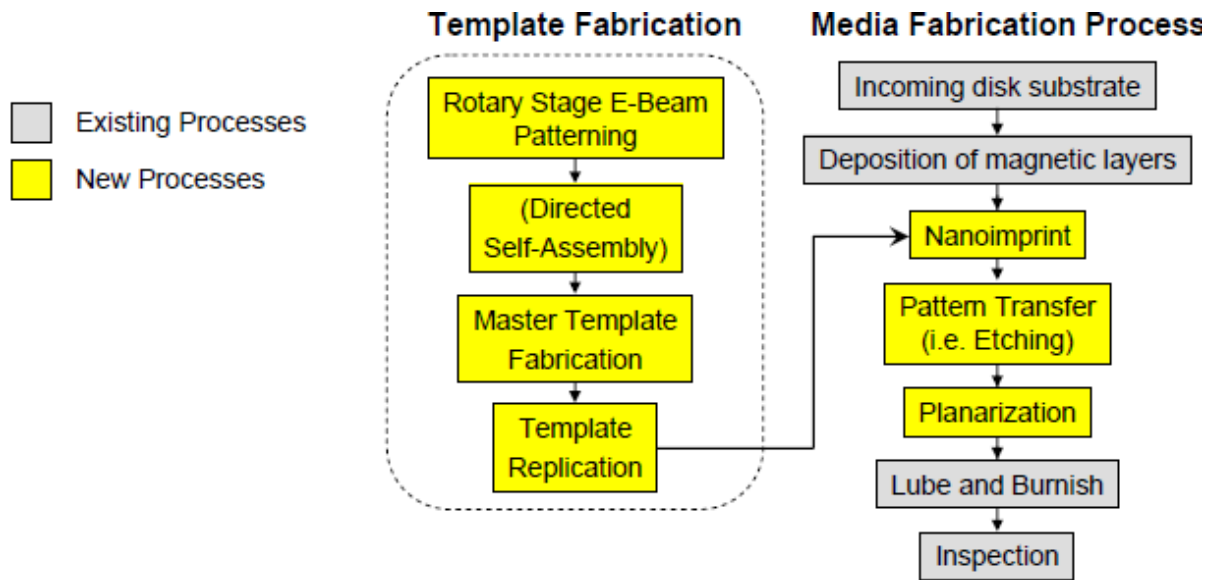


Fig. 3.1. Proposed fabrication plan of BPM [9].

#### 3.1. Structures of Recording Media

Fig. 3.2 shows a schematic view of various functional layers in a typical perpendicular recording medium. In practice, there may be more than one layer involved for every function. Most of the layers in a hard disk medium are deposited by sputtering process. Each functional layer can be described as follow: [26], [27]

1. Substrate (~ few mm). The recording medium is typically AlMg alloy pre-coated with a NiP layer or a glass substrate. Server and desktop HDDs have disk substrates with an outer diameter of 3.5", while HDDs for laptops have disks with an outer diameter of 2.5". Other form factors such as 1.8 and 1" are also common in consumer electronics (CE) applications such as MP3 players. HDDs with 1.3" disks are also being considered to compete with the flash drives in the CE market. Prior to the

deposition of any layer, the substrates are cleaned to remove chemical and particle contaminants.

2. Adhesion layer (~10 nm). This layer – made of Ta, Ti, or an alloy of these materials – helps in improving the adhesion of SUL and all the other layers with the substrate.
3. Antiferromagnetic layer, made of IrMn or FeMn, is used to exchange-bias SUL. By biasing, SUL will have single domain and the easy axis of magnetization towards the radial direction. This is meant for minimizing spike noise from SUL.
4. SUL (~80 nm, with antiferromagnetic layer), which is a stack of SUL 1/Ru/SUL 2. SUL 1 and 2 is each a CoTaZr layer, which helps in conducting the flux from the writing pole of the head to the trailing pole. The antiferromagnetic coupling will minimize remanence and magnetostatic energy of SUL and thus lower the noise during reading process.

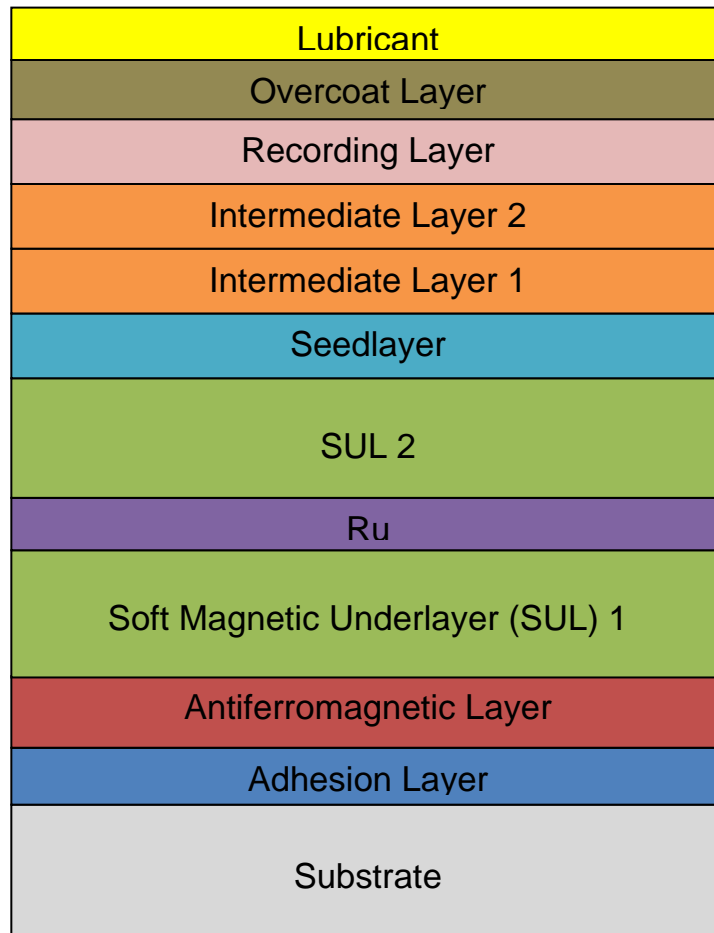


Fig. 3.2. Functional layers of perpendicular recording medium. Layers are not to scale [27].

5. Seedlayer. It is made of Ta and used for better crystallographic control of the recording layer.
6. Intermediate layer/IL (~ 20 nm, with seedlayer). IL 1 is made of Pd/Ru and used to provide epitaxial growth conditions for the recording layer. Seedlayer will enhance this preferred growth. For perpendicular media with Co-based recording layers, it is essential to obtain grains with a Co[0002] orientation perpendicular to the film plane. Therefore, the intermediate layer should have the fcc(111) or hcp(002) texture. IL 2 is made of Ru and used to control grain segregation, and thus controlling the coercivity ( $H_c$ ). IL as a whole serves to exchange-decouple the SUL and the magnetic layer, thus reducing the noise of the recording medium.
7. Recording layer (~15 nm). Typically, CoCrPt:SiO<sub>2</sub> is used. The function is to store information for a long period, typically 10 years, and to produce the read-back signal.
8. Overcoat layer and lubricants (~ 4 nm). Both serve to prevent the disk from failures due to chemical reactions or mechanical impacts (head-disk collision). Overcoat layer is typically amorphous carbon (a-C).

### 3.2. Template Fabrication

In BPM, we need a feature size of 10-25 nm period with a precision tolerance of 5%. Electron beam lithography (EBL) can fulfill this requirement. However, EBL is a serial process so that using EBL alone will consume much time and cost. On the other hand, self-assembly process is relatively more efficient and cheaper in the expense of worse precision tolerance.

Combination of top-down and bottom-up techniques, i.e. EBL and self-assembly process, can offer small feature size and high precision with low cost and high efficiency. For BPM application, chemical pre-patterning is more suitable than graphoepitaxy because it can give high-quality stringent pattern without compromising the storage area [28]. Here chemically-assisted self-assembly process will be used to obtain feature density multiplication and pattern quality rectification as shown in Fig. 3.3.

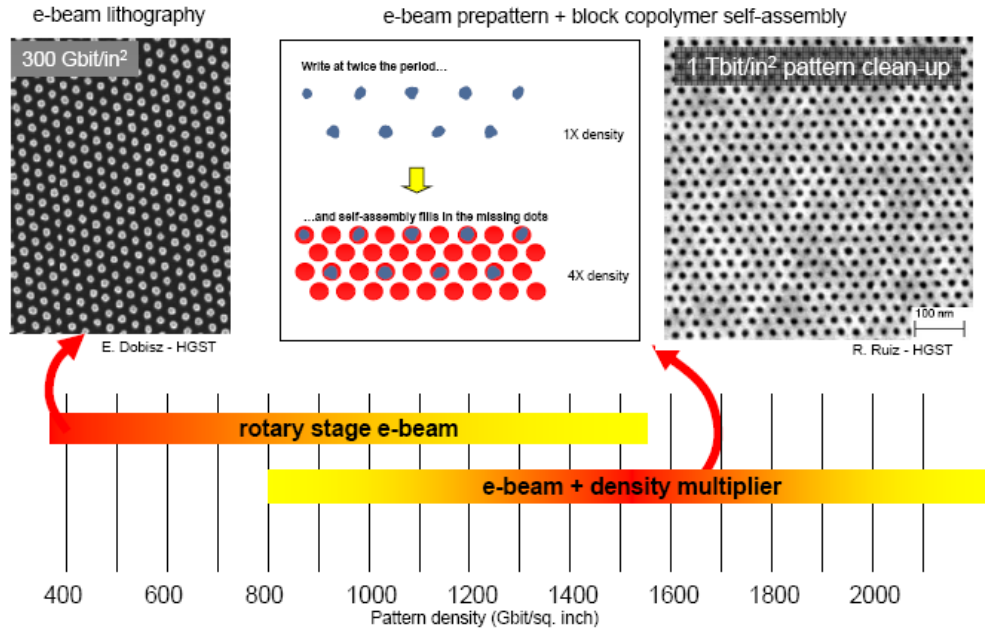


Fig. 3.3. Chemically-assisted pattern generation [9].

Self-assembly process of BCP alone is lack of control of orientation and ordering of microdomains. Chemically patterned substrates with length scales comparable to the natural periodicity of the BCP can be used to precisely register various microdomains of BCP. Commensurability and chemical affinity of the microdomains to the patterned substrate play important roles. In the self-assembled process of BCP on chemically patterned surface, commensurability between the natural length scales of BCP system and the periodic pattern on a substrate must exist in order to induce recognition of the pattern on the substrate by the polymer as well as accurate replication. It is found that for BCP adsorption from solution, the stripe width  $L$  must satisfy the limits of  $D < L \leq L^*$ , where  $D$  is the correlation length of an adsorbed blob of similar chain segments, and  $L^* \approx 2N_n\delta^{2/3}a$ , where blocks of length  $N_n$  segments of size  $a$  are adsorbed with a surface energy  $k_B T \delta$  per segment (Appendix 1).

The investigation of the effects of both commensurability and chemical affinity on the registration of lamellar BCP has also been conducted in the stripes of polymer brush and a hydrophilic surface, by varying degree of commensurability ( $L_0/L_s$ ) and the ratio of PS-r-PMMA stripes on the substrate. The results of the SEM examination are shown in Fig.

3.4. It can be seen that the chemical affinity of the substrate improves the registration of the lamellar PS-*b*-PMMA. For chemically neutral stripes, PS-*r*-PMMA with ratio 50:50, the registration of the lamellar PS-*b*-PMMA is limited even when  $\delta \sim 1$ . While for very high affinity (100% PS stripes), the defects are less pronounced and the window for good patterning registration is wider.

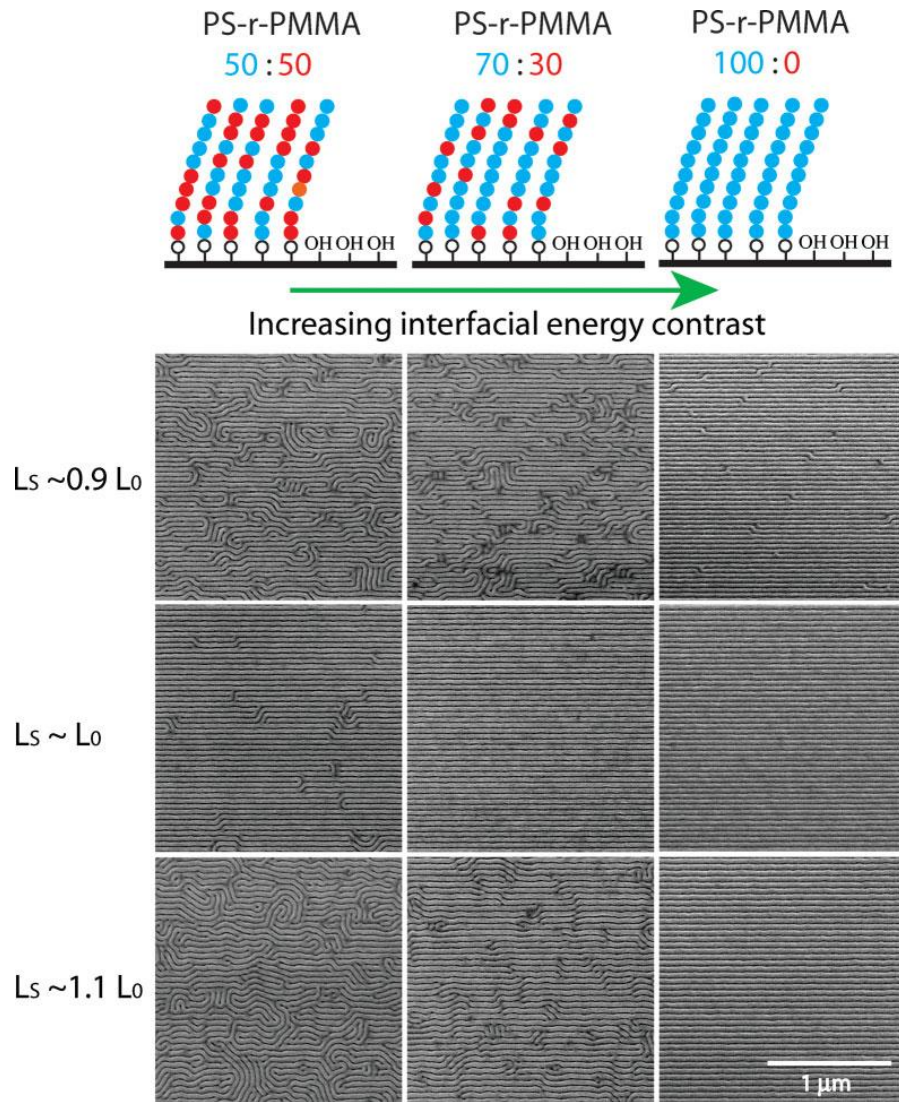


Fig. 3.4. SEM images of lamellae-forming PS-*b*-PMMA block copolymer films ( $L_0 = 48$  nm) on chemically nanopatterned substrates as a function of  $L_S$  ( $L_S = 42.5$  nm,  $47.5$  nm, and  $52.5$  nm) and composition of the random-copolymer brush used to create the chemical pattern. The blue beads represent PS units and red beads represent PMMA units in the random block copolymer brush layer. Higher percentages of PS in the random block copolymer brush produce the higher chemical contrast of the surface patterns to PS-*b*-PMMA. Stronger chemical contrast favors replication of the underlying pattern [29].

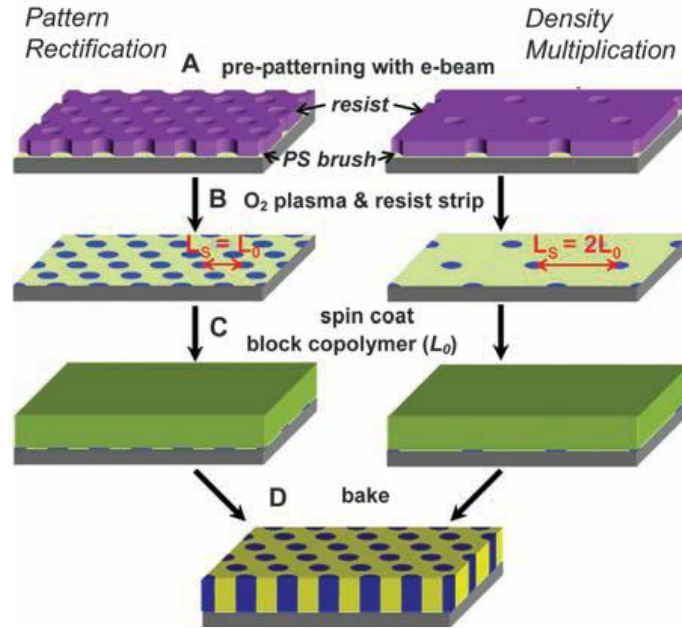


Fig. 3.5. Process to create lithographically defined, chemically pre-patterned surfaces, and subsequent directed assembly. (A) Electron-beam lithography patterns at  $L_S = L_0$  (left) and  $L_S = 2L_0$  (right). (B) Chemical contrast on the substrate after  $O_2$  plasma exposure on the e-beam-defined spots above. (C) Block copolymer thin film. (D) Guided self-assembly in registration with the underlying chemical pattern [28].

The chemically-assisted pre-patterning process is shown in Fig. 3.5. First, rotary-stage electron beam lithography (EBL) is used to pattern the resist on top of the substrate. Rotary-stage EBL is chosen because it can define concentric layouts as required in hard disk media. Rotary-stage EBL is capable of fabricating grooves and bits on narrow pitch in concentric arrays with sub-50-nm range [30]. The schematic of rotary-stage EBL for creating concentric patterns on master template is given in Fig. 3.6.

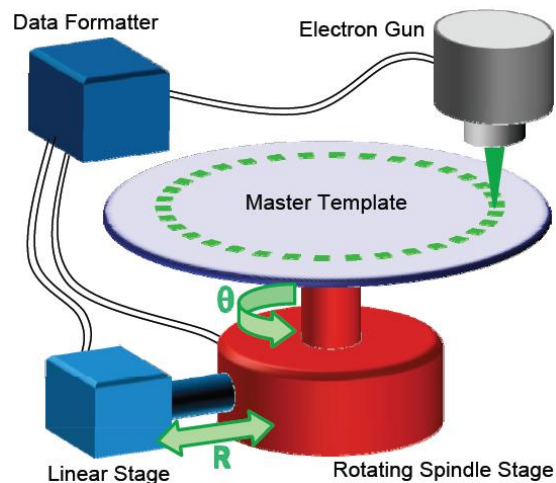


Fig. 3.6. Rotary-stage EBL [22].



In this process, the servo patterns are also written simultaneously with the data patterns. The continuous stage movement flyback lithography (CSFL) of rotary-stage EBL is capable of working in conjunction with a blankingless beam shift lithography (BLSL). This combination is very effective for fabricating various kinds of servo pattern elements. The layout of servo patterns can be seen in Fig. 3.7. Servo patterns are included on hard disks to enable the head element to read and write data at precise locations. We need to write the servo patterns only once in the master template, thus eliminating the need for servo writing in subsequent processes [22]. The disk is then exposed to oxygen plasma. Upon removal of the resist, a chemical contrast on the substrate is obtained.

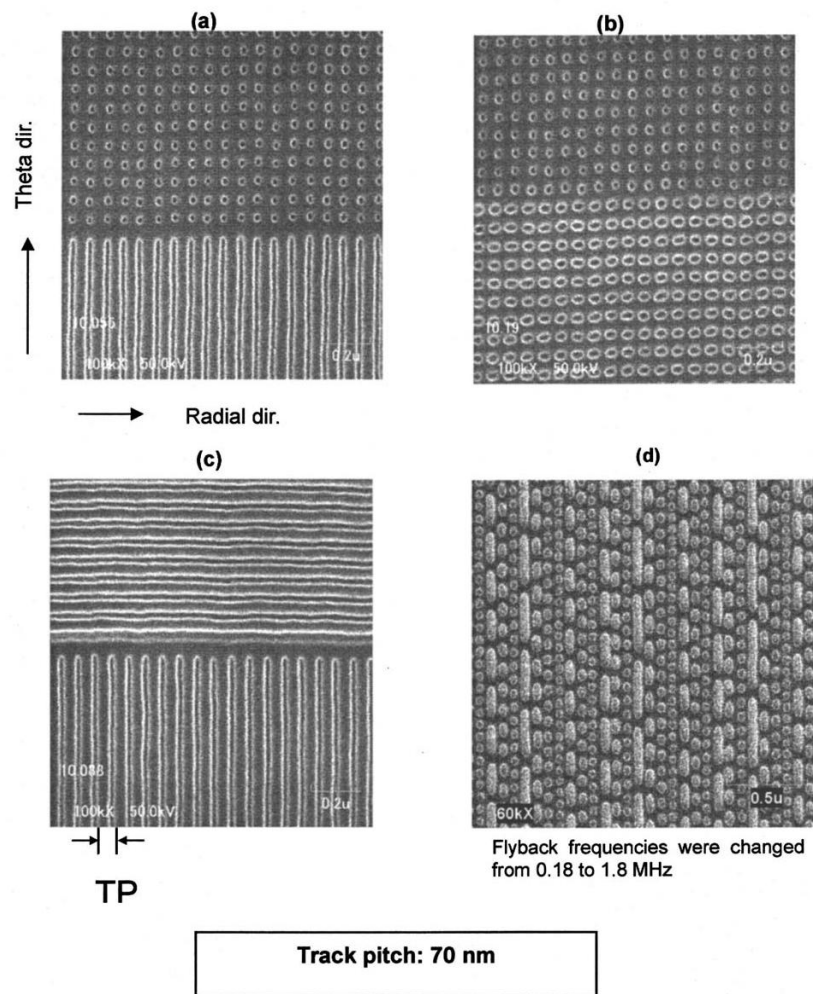


Fig. 3.7. Servo pattern element write using the CSFL function. (a) Groove and dot, (b) dot and shifted elliptical dot, (c) groove and right-angled groove, and (d) different-length pits with various doses [30].

One important thing is that for a constant spin speed, the outer part of the media will

move with larger linear velocity. This implies that the data rate will be larger at the outer part. To resolve this, the bit size must vary with radius, i.e. larger bits for increasing radius. This requirement is easily accomplished in EBL system.

The bottom-up process begins by spin coating block copolymer (BCP) film onto the substrate. The ultimate resolution ( $R$ ) expected in this process is basically proportional to the domain period  $D$  of BCP film. For BCP lithography purpose, we have to be in the strong segregation limit ( $\chi N \gg 10$ ). In this region, the domain period is given by  $D \sim aN^{2/3}\chi^{1/6}$ , where  $a$  is the segment length,  $N$  is the overall number of segments (monomers), and  $\chi$  is the Flory-Huggins interaction parameter. However,  $D$  is the period or the sum of the characteristic length scale of the BCP domains (PS and PMMA in our case). Since one domain is selectively etched away, the resolution will be the volume fraction of PS or PMMA (whichever is smaller) times the period. Theoretically, BCPs may form ordered periodic structures at the molecular scale ranging from 5-50 nm [31].

For BPM application purpose, it is required that the BCP lithography process has high resolution. Therefore, it is necessary to choose BCP with a high  $\chi$  and decrease the block length ( $N$ ) [32]. The resolution will also depend on etch selectivity between the blocks and subsequent pattern transfer process. It is required that the BCP has cylindrical or spherical morphologies. The morphology of BCP is determined by the volume fraction of each block, the relative chain-length differences of the constituent copolymers, and the processing condition. [33].

PS-b-PMMA has been widely used due to excellent chemical selectivity between PS and PMMA blocks, smooth microphase separation, the same glass-transition temperature, and a wide range of available solvents [34]. However, now PS-b-PDMS has also been considered since it has a high  $\chi$ , giving a large driving force for microphase segregation, and a high chemical selectivity between the two blocks [35].

As shown in Fig. 3.8, the BCP film is annealed in vacuum to obtain cylindrical PMMA morphologies in PS matrix. The self assembly process of PS-b-PMMA is guided by the pre-patterned template, which is created by e-beam, to create a long-order pattern. The PMMA block will preferentially wet the spots exposed to oxygen plasma while the PS block will be slightly attracted to the background areas. The PMMA domains can then be selectively etched. This self-assembly process will increase the resolution of e-beam features by a factor of four and reduce the needed exposure time.

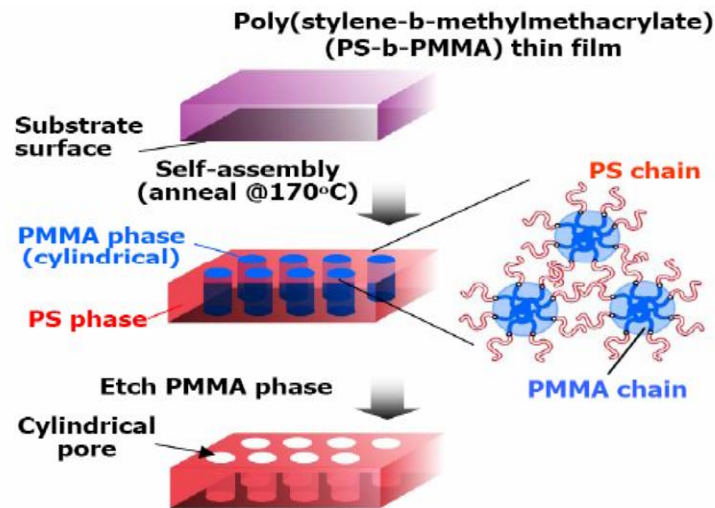


Fig. 3.8. Self-assembly of block-copolymer [9].

In HDD industry, we need to produce millions of disks. One method that provides simplicity, low cost, and high throughput is nanoimprint lithography (NIL). However, in imprinting such high volume of disks, the template can be easily damaged. Thus, template replication is essential to extend the template lifetime. Before proceeding to the media fabrication step, the obtained master template is first replicated by UV-NIL followed by a plasma-based transfer process into thousands of thin silica molds. These silica molds are then used in UV-NIL process to produce the disks.

### 3.3. Media Fabrication

To achieve high throughput, double-sided patterning is carried out using NIL. In UV-NIL process, as shown in Fig. 3.9, a layer of resist is sprayed on the substrate and the thin silica mold is brought into intimate contact with the substrate. To ensure intimate contact,

the template is bowed so that its center forms an initial contact with the center of the substrate. Then, capillary force will pull the entire template into conformal contact with the disk. Upon exposure to UV light, the imprinted resist will crosslink. Examples of patterned structures resulted from UV-NIL process are given in Fig. 3.10.

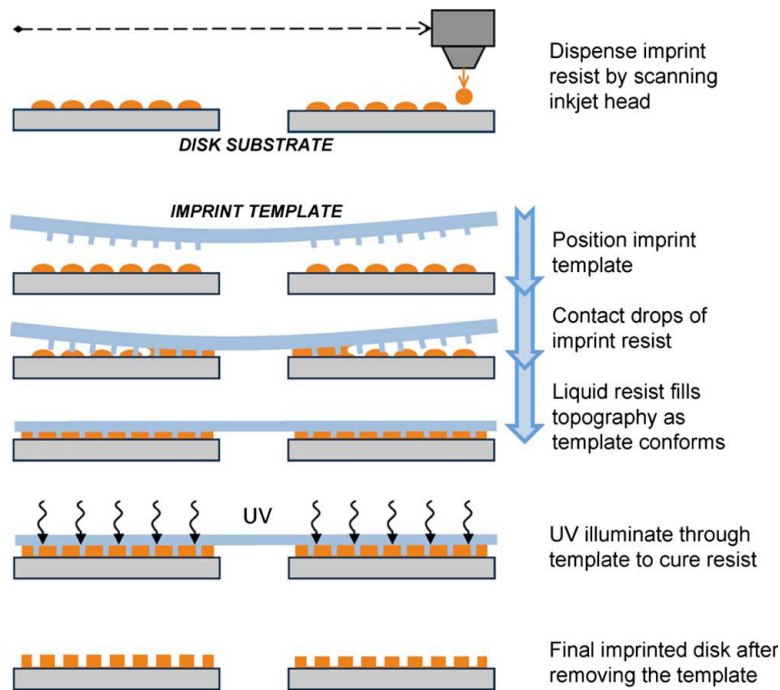


Fig. 3.9. UV-NIL process for patterned media [22].

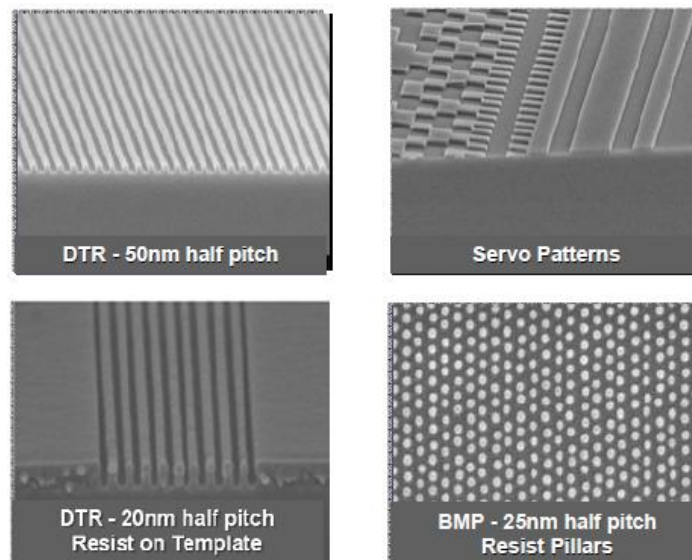


Fig. 3.10. Patterned media imprint examples [36].

The next step is then to transfer the pattern to a magnetic film. The magnetic film must be thin (<20 nm) for the write and read head to be able to resolve the high density islands. There are two generic approaches to this pattern transfer: [20]

- (1) pre-patterning a substrate and subsequent deposition of a magnetic film;
- (2) depositing a magnetic film and then dry-etching or milling it through a mask to define the islands.

It is also possible to use a lift-off process where the magnetic film is deposited onto the patterned resist and then the unwanted parts are dissolved to leave isolated magnetic islands. However, lift-off has not been particularly successful at sub-10 nm dimensions.

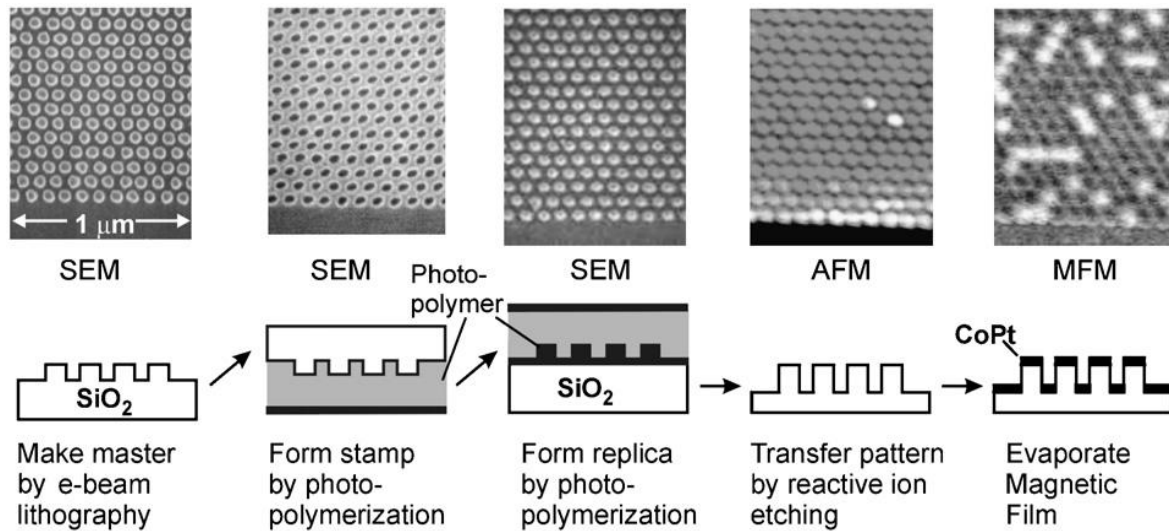


Fig. 3.11. Steps in the fabrication of patterned magnetic media [20].

The approach of pre-patterning a substrate, as shown in Fig. 3.11, has probably been the front running approach to date. The main motivations for using the pre-patterning substrate were:

- (1) no good reactive ion etching (RIE) chemistry was known for the magnetic materials of interest;
- (2) ion milling tends to result in redeposition;
- (3) it would be necessary to clean all resist and redeposition to produce a clean, flyable disk;

(4) pre-patterning the substrate puts the patterning process earlier in the manufacturing process, and thus minimizing the impact of lower yields.

This approach has progressed significantly, with published patterned densities of 300 Gb/in<sup>2</sup>, the growth of thin perpendicular anisotropy layers, an understanding of the reversal processes, and static tester recording studies. However several challenges still exist. First, magnetic material in the trenches can give rise to noise. Second, the trenches also affect the stabilities in the flying. Moreover, there have been significant progresses in the RIE of magnetic materials and ion beam etching technology. So magnetic film etching is receiving renewed interest. At this time, the question of how to best pattern the magnetic film is still open.

For high-density recording, the head must fly within a close distance above the media. The magnetic spacing requirements for increasing areal density are illustrated in Fig. 3.12. BPM process creates topographies and thus imposing a high probability for the head to collide with the surface. Therefore, planarization scheme is introduced. First, a non-magnetic material is deposited by CVD or sputtering. Then, to obtain a planar disk surface, dry etching or milling can be used. Spin deposition and etch back can also be an option. However, it results in poor uniformity from the disk inside-diameter (ID) hole. Another alternative is using chemical mechanical polishing (CMP). CMP is a very mature process, but wet chemistry and consumables are problems. A planar disk is also advantageous in the overcoat process.

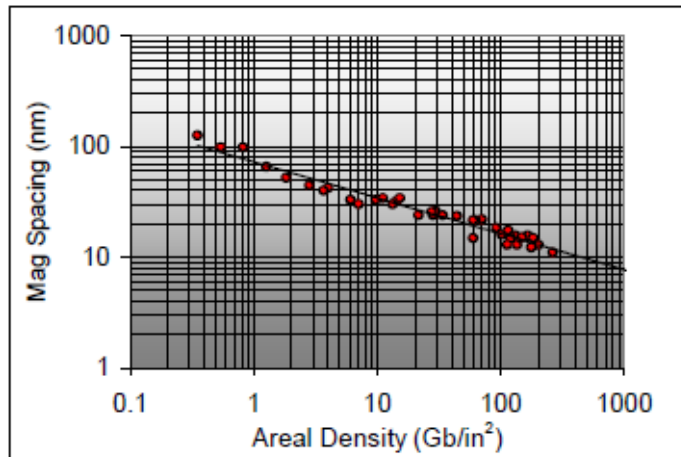


Fig. 3.12. Magnetic spacing requirements for HDD [4].

According to Hitachi and Seagate, the overall proposed schemes ensure high resolution and high throughput. Molecular Imprint Inc. claims that each of their NIL tools can produce millions of disks with only a single master template, as illustrated in Fig. 3.13. In their scenario, one master template can be faithfully replicated into 10,000 silica daughter templates, each of which can reproduce 10,000 disks. It is worthwhile to mention, however, that this estimation has not been proven in real industry.

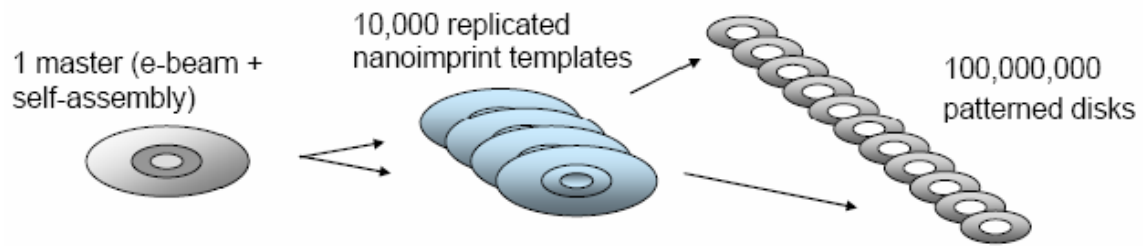


Fig. 3.13. Illustration of high throughput disk fabrication with the proposed fabrication plan [9].

## 4. Market Opportunity

### 4.1. Technology Supply Chain

In order to understand the importance of our technology, it is essential to locate the position of recording media in HDD process chain. The HDD supply chain is illustrated in Fig. 4.1.

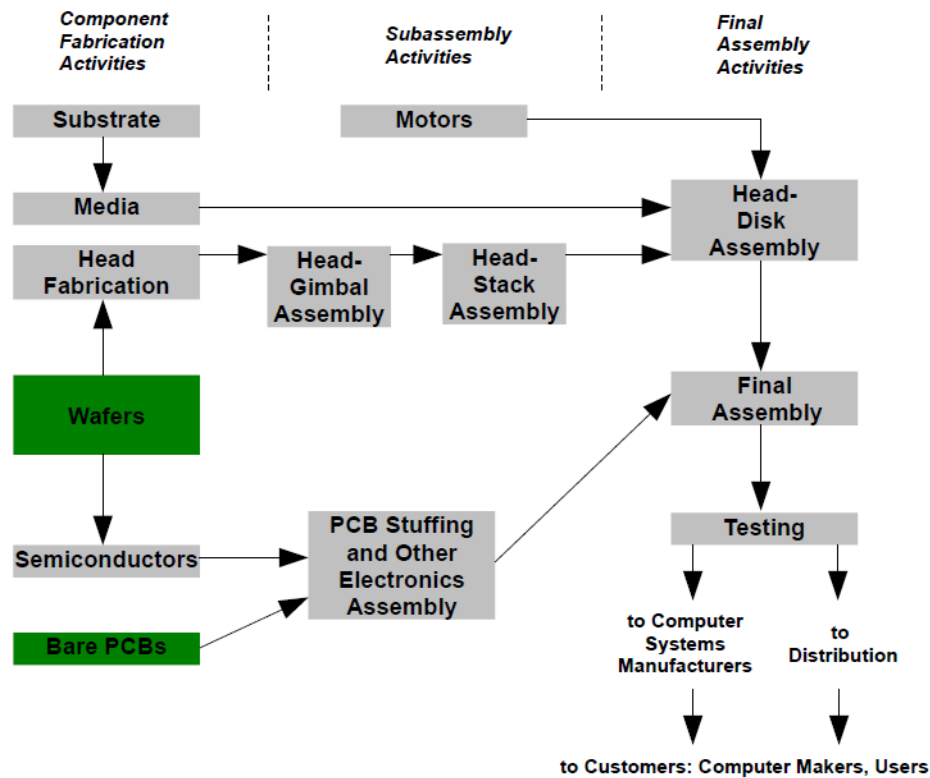


Fig. 4.1. HDD supply chain [37].

A typical HDD manufacturing process starts with the fabrication of media, head, electronic components and motors. Through the various assembly steps, all the components are integrated into commercial products to be used in computers, telecommunication equipments, and other electronic devices. The BPM technology will play a role in the fabrication of the media. With the capability of meeting consumers' demand of high-density recording, an investment in this area is promising to gain significant profit.

The globalization of HDD supply chain can be seen in Fig. 4.2. It is important to note that the HDD media are mainly fabricated in USA, Malaysia, and Singapore.



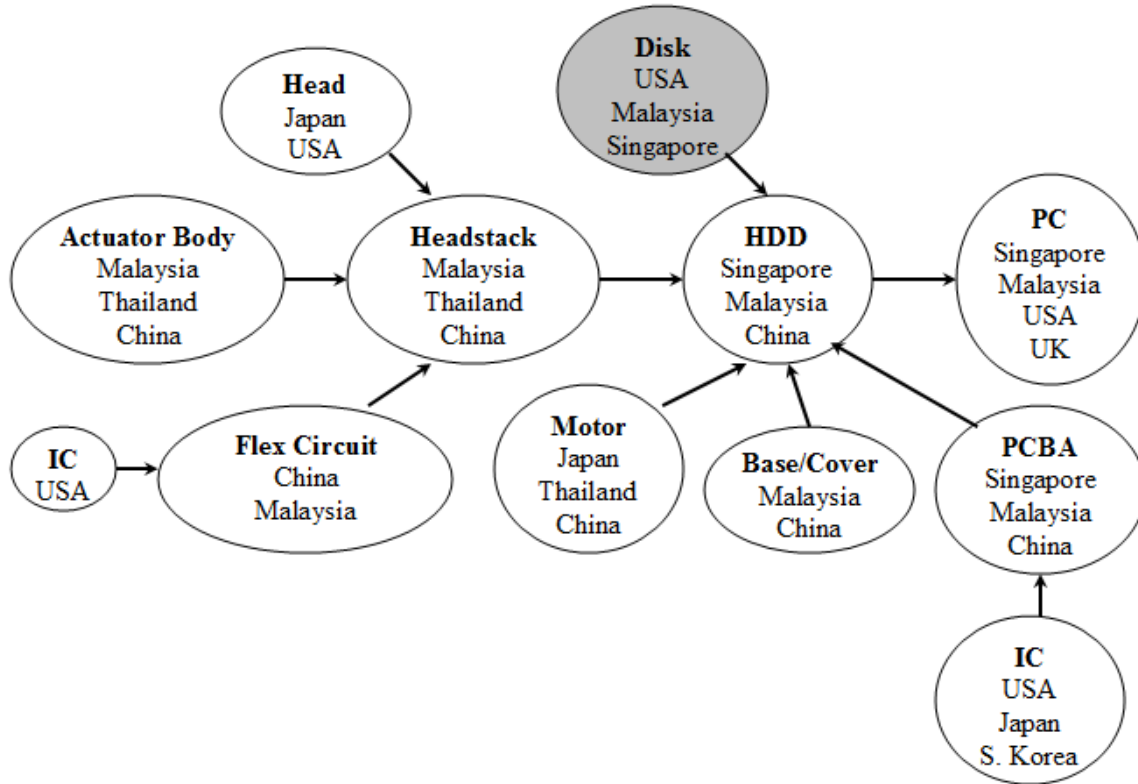


Fig. 4.2. Globalization of HDD supply chain [38].

## 4.2. Competing Technologies

In order to achieve areal densities higher than PMR, besides using BPM as new recording media, we can use write-assist method to write in materials with a very high anisotropy. Several write-assist methods have been proposed, such as heat-assisted magnetic recording (HAMR), microwave-assisted magnetic recording (MAMR), and exchange-coupled composite (ECC) media [39]. All these write-assist methods are based on the same concept, i.e. enabling higher  $K_U$  to enable smaller grain and thus better signal-to-noise ratio (SNR).

### 4.2.1. Heat-Assisted Magnetic Recording

HAMR uses localized heat energy to reduce the medium coercivity. Its principle is similar to magneto-optical recording [40]. In this technology, we introduce write temperature as a new degree of freedom. Writing in media with higher anisotropy is made possible by using a laser to heat the recording layer up to slightly below  $T_C$  (Curie temperature) where

the coercivity is lowered below the available applied magnetic field. The written region is then rapidly frozen during the cooling process. The media can then be stably stored in room temperature. This writing process of HAMR is illustrated in Fig. 4.3.

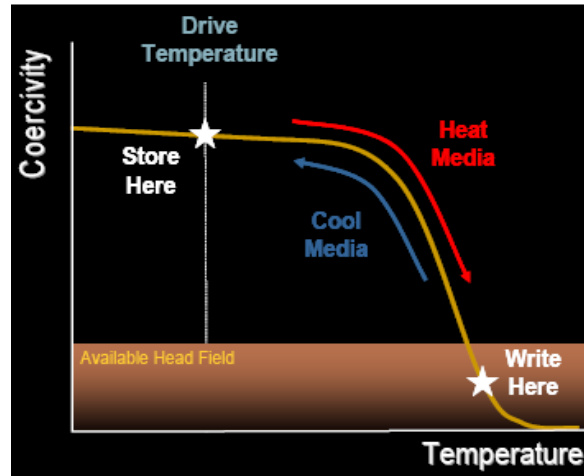


Fig.4.3. Diagram of HAMR writing process [41].

However, there are several challenges faced by HAMR. First, at  $T_C$ , the media grains are paramagnetic and do not respond to a field. This phenomenon is known as superparamagnetic trap. As the grains cool down from  $T_C$ , the magnetization fluctuates rapidly. If the cooling rate after initial heating is too fast, the magnetization will be quenched in an arbitrary state. On the other hand, if the cooling rate is too slow, thermal erasure will increase due to heat that diffuse to neighboring bits [42]. Thus, temperature dependence of the medium magnetic properties, particularly around  $T_C$ , is crucial for recording rate limitations and recording quality in HAMR. Factors that limit the rate of magnetization collapse and reformation along with the quality of the magnetization formation during freezing should be well understood. Recording simulations are needed to answer those questions.

The second and the ultimate challenge is breaking the diffraction limit of the laser source. In optical data storage, diode lasers have been widely used because they are inexpensive and capable of emitting high-power coherent light. The problem here is that those diode lasers available have wavelengths ranging from several hundred nanometers and longer.

State-of-the-art diode lasers are available at 375nm wavelength. However, to obtain storage densities beyond  $1\text{Tb}/\text{in}^2$ , we need spot size  $< 50\text{nm}$  [43]. The diffraction limit of far-field optics would provide achievable spot sizes that are too large. Thus, near-field optics has to be used [42]. In addition, an efficient technique must be provided for delivering large amount of light power to the recording medium and confining the light to sufficiently small optical spots. Finally, all the optical parts should be coupled for a complete optical system.

There are also challenges associated with building an integrated head for HAMR, lubricant, overcoat, and head-disk interface tribology due to high operating temperature.

#### 4.2.2. Microwave-Assisted Magnetic Recording

In MAMR, an *ac* field with microwave frequency is applied along the easy axis opposite to the initial magnetization as shown in Fig. 4.4. The ferromagnetic resonance (FMR) frequency of the grain is determined by the externally applied reversing field and the anisotropy field of the grain. If the frequency of the *ac* field matches that of the grain, the system will absorb energy from the *ac* field. Above a certain switching field threshold, the magnetization precession will increase its precession angle and irreversibly gyro downwards within the duration of the pulsed reversing field. Thus, MAMR allows recording in the medium with anisotropy field higher than the maximum recording field [44]. As one of the proof of MAMR concept, reduction of switching field of single 20nm Co particle in the presence of an *ac* field has been demonstrated [45].

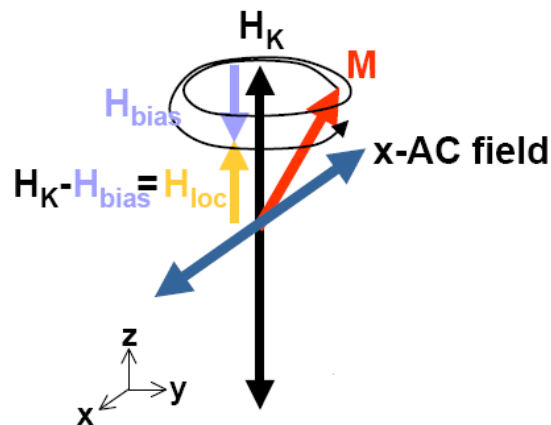


Fig. 4.4. MAMR process [41].

Proposed design of MAMR is illustrated in Fig. 4.5 (a). During the recording process, magnetization oscillation is generated in the field generating layer (FGL), as illustrated in Fig. 4.5 (b). Assuming that the magnetization of the perpendicular layer in the oscillating stack is along its anisotropy easy axis, the magnetization of the FGL is experiencing an effective magnetic field along the perpendicular axis. If the interlayer exchange field is greater than  $4\pi M_S$ , when the spin polarized current is zero, the magnetization will align itself in the perpendicular direction due to the damping torque. However, spin-polarized current will induce spin momentum transfer that generates a torque, termed spin torque, that is antiparallel to the damping torque. At sufficient current density, precession angle  $\theta$  will be achieved. The angular frequency of the magnetization precession is  $\omega = \gamma H_{\text{effective}}$ . Current variation can tune the frequency directly over a very broad range, thus the frequency-current correlation is very important.

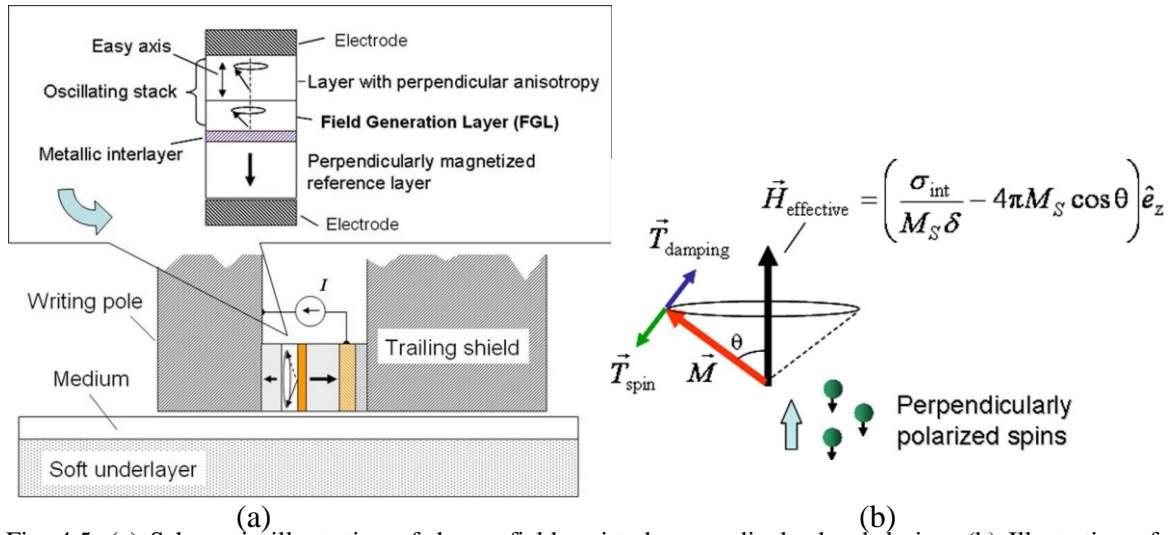


Fig. 4.5. (a) Schematic illustration of the *ac* field assisted perpendicular head design. (b) Illustration of magnetization precession of the field generating layer facilitated by the spin torque.  $\sigma_{\text{int}}$  is the interlayer exchange coupling surface energy density,  $M_S$  is the saturation magnetization, and  $\delta$  is the thickness [44].

There are many advantages of MAMR, such as the direct coupling of assist energy into the magnetization mode and well understood theory behind it. However, MAMR also faces obstacles in its implementation. The device that is embedded in the head has not been proven to be technologically viable yet. Controlling the location of *ac* field and gradient is also a major obstacle in MAMR.

Moreover, according to J. Zhu *et al.*, the optimum value for the switching field reduction is at field angle  $\theta = 30^\circ$ . At this optimum angle, the minimum switching field is  $\sim 1/3$  of the minimum switching field in the absence of *ac* field (Stoner-Wohlfarth value). Therefore, MAMR is only able to achieve about three times of perpendicular recording areal density ( $>1.5\text{Tb/in}^2$ ). In the most recent simulation, it was shown that a circular *ac* field of 2.5 kOe peak amplitude and 50 GHz frequency will enable an areal density of  $1.88\text{ Tb/in}^2$  with a medium SNR above 18 dB. The highest obtainable density is  $2.34\text{ Tb/in}^2$  at damping constant of 0.175 [20].

### 4.2.3. Exchange Coupled Composite Media

In ECC, a soft layer is used to assist the switching of the hard layer. Illustration of a grain in an ECC medium is given in Fig. 4.6. This write-assist process, known also as domain-wall-assisted switching, occurs only in the presence of an applied field [39]. The applied field will reverse the magnetization in the soft layer, creating a domain wall within each grain. This domain wall exerts pressure onto the hard layer and thus the switching field will be reduced. Very high anisotropy contrast between the layers is desired. Ideally, by using ECC, infinitely high anisotropy fields can be switched.

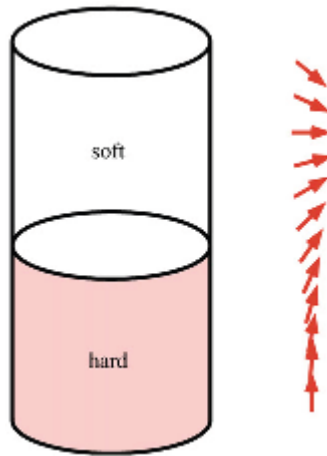


Fig. 4.6. Illustration of a grain in an ECC medium. It consists of a magnetically hard part and a magnetically soft part [39].

Fig. 4.7 depicts a schematic of the layer and magnetic structure for the proposed ECC media.  $[\text{Co-PdSiO}]_n$  is used as the hard layer and FeSiO acts as the soft layer with a non-

magnetic PdSi interlayer between the hard and soft layer to tune the exchange coupling. SiO was doped into Pd layer to get magnetically isolated grains.

Advantages of ECC media compared to conventional continuous media are: 1) writability could be significantly improved without compromising its thermal stability; 2) the switching field of the media is much less sensitive to the angle dispersion (angle between the easy axis and applied field) compared to the perpendicular media. It is necessary to conduct further research to find out a better combination of hard and soft layer and optimize relevant magnetic parameters such as thermal stability and switching field to reach areal density beyond 1 Tb/in<sup>2</sup>.

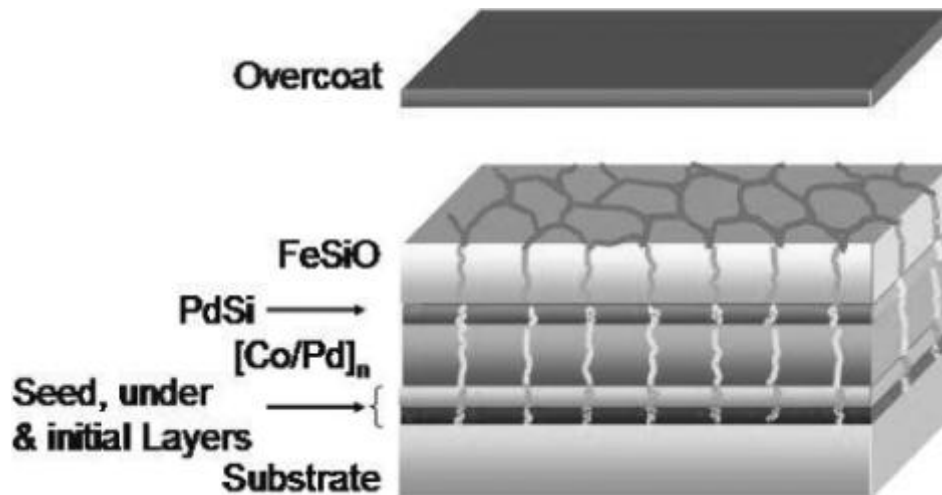


Fig. 4.7. Basic structure of proposed ECC media [46].

#### 4.2.4. Comparison among HAMR, MAMR, and ECC media

Among those three write-assist methods, HAMR is the most extensively studied. MAMR and ECC media are still in the infancy of their development to be currently considered as feasible manufacturing options. HAMR might enter the market before BPM, thus threatening the potential of commercializing BPM technology.

However, BPM can be combined with HAMR and ECC systems [24]. Magnetic isolation and small size distribution in BPM will enhance the HAMR and ECC areal density capabilities. By using a matrix with low heat conductivity, BPM can control heat

diffusion and thermal fluctuation in HAMR, thereby resolving the problem of erasure of information on adjacent tracks and recorded bit instability. Meanwhile, in ECC, the completely isolated magnetic grains in BPM will help totally eliminate the exchange coupling between magnetic grains. Thus, even if HAMR or ECC is established first, we can still use our media in their systems. The combination of HAMR with BPM is even projected to reach an areal density of  $\sim 100 \text{ Tb/in}^2$  based on the thermal stability of known magnetic materials [47].

#### 4.2.5. Outer Competitor

In the market, besides HDD, there are still many other types of storage disks. Solid-state drive (SSD) has especially gained commercial success due to its high speed, low noise, and low power consumption. However, as can be seen in Fig. 4.8, HDD offers the best areal density, capacity, and cost. Therefore, HDD shipment volume can be predicted to continue being on top as long as it can fulfill the increasing demand of areal density and capacity while maintaining its low cost.

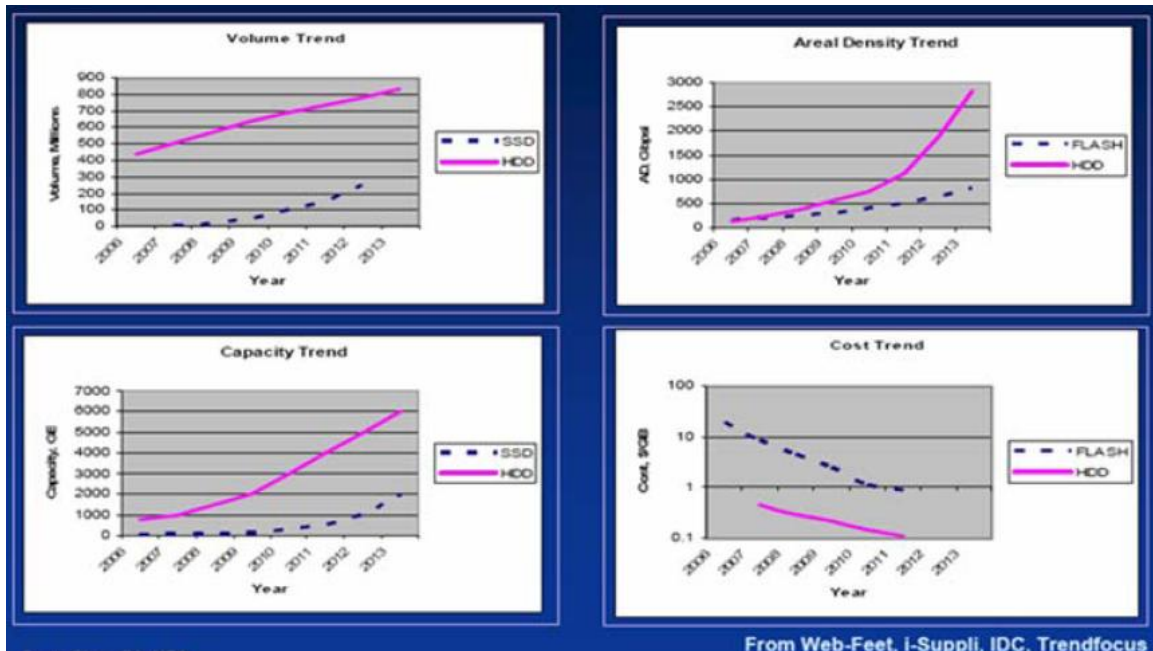


Fig. 4.8. Comparison between HDD and SSD [36].

### 4.3. Complementary Technologies

#### 4.3.1. Head Technology

The recording and reading process in BPM is different from that of PMR. Reading the data faithfully from such small bits is challenging. For example, the head must fly within a reasonably close spacing from the media to resolve the high-density media, while at the same time maintain a safe distance to avoid collisions with the media due to protrusions and dust. To solve this problem, planarization process is inserted in the fabrication process. In the area of the read sensor, significant advances will be required for Tb/in<sup>2</sup> applications. Challenges faced by read head are summarized in Table 4.1. The geometrical requirements for read head at high density are further listed in Table. 4.2.

Table 4.1. Read head challenges [4].

<b>Small Geometry</b>	Track width
	Shield spacing
<b>High Sensitivity (mV/Oe)</b>	$\Delta V = i \eta (\Delta R/R) R$
<b>Low Noise</b>	Johnson noise
	Shot noise (TMR)
	Magnetic noise
<b>Design Constraints</b>	$50 \Omega < R < 500 \Omega$
	Temperature Rise
	Breakdown Voltage
	Spin Torque Instability
	Magnetic Self-Field


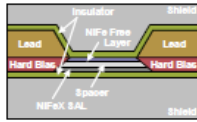
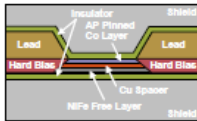
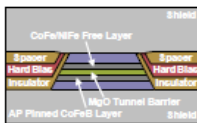
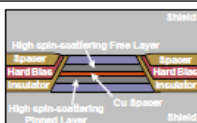
Table 4.2. Geometrical requirements for head for patterned media [4].

Requirement	300 Gbit/in <sup>2</sup>	500 Gbit/in <sup>2</sup>	750 Gbit/in <sup>2</sup>	1000 Gb/in <sup>2</sup>	2000 Gb/in <sup>2</sup>
Track Width	60 nm	45 nm	35 nm	27 nm	20 nm
Shield Spacing	35nm	32nm	30nm	22nm	20nm
SNR	33 dB	32 dB	31 dB	30 dB	30 dB

To fulfill these requirements, head technology has been evolving from CPP TMR to CPP GMR, as illustrated in Fig. 4.9. The structure of CPP TMR and CPP GMR are basically similar, except that the CPP GMR uses non-magnetic metal such as Cu instead of oxide as the interlayer between two ferromagnetic layers. The current CPP TMR sensor is based on spin-dependent tunneling mechanism. As the areal density increases, the sensor



size must shrink. This will impose very high resistance. Fig. 4.10 shows the trends of data transfer rate for high-end HDD systems and allowed resistance-area product ( $RA$ ) of read head sensors with a CPP structure versus areal density. As shown, in order to increase the data transfer rate for higher areal density recording,  $RA$  must be reduced accordingly. This fact indicates that the TMR head, with a predicted minimum achievable  $RA$  value of  $1 \Omega\mu\text{m}^2$ , will reach a limit at about  $300 \text{ Gb/in}^2$ . On the other hand, CPP GMR structure which uses a metallic spin-valve is a reliable candidate for much higher areal densities because it can achieve a minimum  $RA$  of about  $0.1 \Omega\mu\text{m}^2$ .

Year	Areal Density	Sensor Technology	Structure	MR Effect	Current Geometry	Major Noise Sources
1979	10 Mb/in <sup>2</sup> (LMR)	Thin-film Inductive		N/A	N/A	Barkhausen Johnson
1991	100 Mb/in <sup>2</sup> (LMR)	MR Sensor		Anisotropic MR	CIP (Current In Plane) Lead Lead	Johnson
1997	2 Gb/in <sup>2</sup> (LMR)	Spin Valve		Giant MR	Bottom Shield	Johnson
2006	100 Gb/in <sup>2</sup> (PMR)	Tunnel Valve		Tunneling MR	CPP (Current Perpendicular to the Plane) Shield	Johnson Shot Noise Mag Noise
2011	1 Tb/in <sup>2</sup> (PMR)	CPP GMR		Giant MR	Shield	Johnson Mag Noise Spin Torque

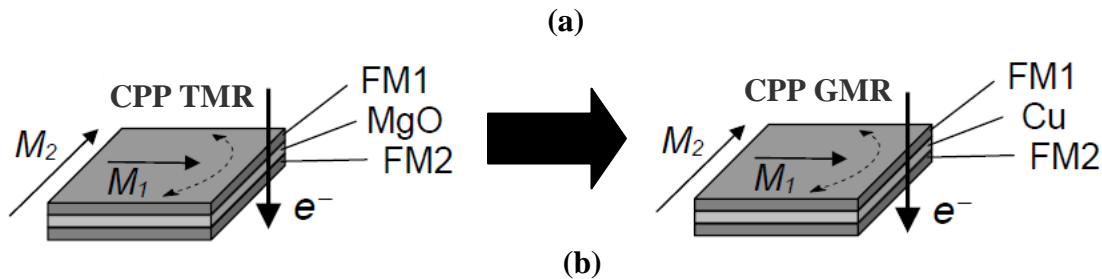


Fig. 4.9.(a) Evolution of head technology; (b) Structure of CPP TMR and CPP GMR heads [4].

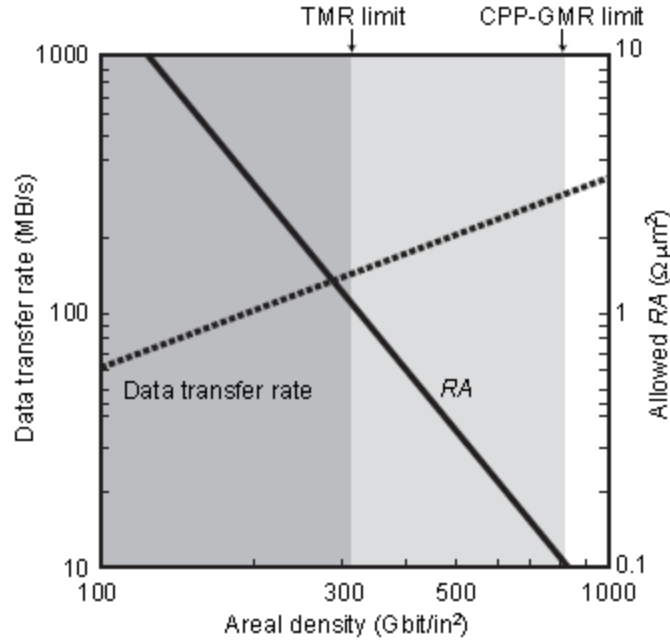


Fig.4.10. Trends of data transfer rate for high-end HDD systems and allowed resistance-area product ( $RA$ ) of read head sensors with CPP structure versus areal density [48].

CPP GMR is then projected to be applied for  $1\text{Tb/in}^2$  areal density around 2011. In CPP GMR, since the spacer layer is conductive and the current flows in a direction perpendicular to the plane of the layers, the overall electrical resistance, or sheet resistance, is extremely low. This result in a  $\Delta RA$  that is too small to achieve a sufficiently high signal-to-noise ratio (SNR). Fig. 4.11 shows the required  $\Delta RA$  of the CPP-GMR for various recording densities as estimated for the following parameters: output signal voltage for sufficient SNR = 1.5 mV, head efficiency = 30%, sense current density =  $100\text{ MA/cm}^2$ , power consumption of sensor element = 0.6 mW. One special feature of the CPP-GMR is that the absolute  $\Delta R$  value increases as the sensor size decreases. Therefore, the required  $\Delta RA$  becomes smaller as the recording density approaches  $300\text{ Gb/in}^2$ , where the power consumption of the sensor is the dominant factor in limiting the sense current. Meanwhile, the current density limit becomes dominant over  $300\text{ Gb/in}^2$ , saturating the required  $\Delta RA$  to be about  $5\text{ m}\Omega\mu\text{m}^2$ .

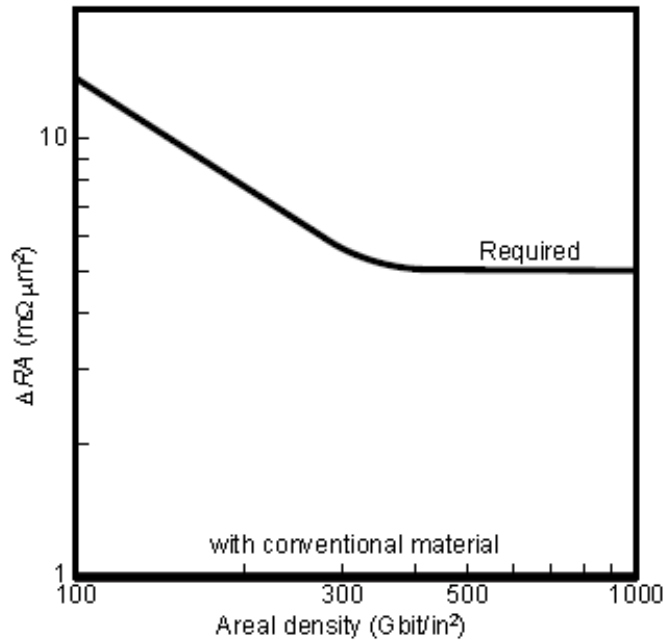


Fig 4.11. Estimated required  $\Delta RA$  of CPP-GMR for higher recording densities for output signal voltage = 1.5 mV, head efficiency = 30%, sense current density = 100 MA/cm<sup>2</sup>, power consumption of sensor element = 0.6 mW [48].

Several methods have been described to enhance the CPP-GMR, such as

1. To use a novel synthetic ferrimagnet pinned-layer structure in CPP spin-valves. This structure will effectively enhance the  $\Delta RA$  while maintaining a high magnetic pinning field.
2. To use newly developed high-resistivity ferromagnetic alloys for the free and reference layers.

The high  $\Delta RA$  of 7.7 mΩμm<sup>2</sup> was achieved in a fully metallic CPP-GMR element with an  $RA$  of around 0.1 Ωμm<sup>2</sup> by using high-resistivity, high spin-asymmetry coefficient materials such as Co-Fe-Al. These materials will enable an areal density ~1 Tb/in<sup>2</sup>.

CPP-GMR sensors with an Al<sub>2</sub>O<sub>3</sub> current-confined-path (CCP) insertion layer in the Cu spacer have also been investigated. A  $\Delta RA$  product of 30 mΩμm<sup>2</sup> was demonstrated for devices with dimensions of 50 x 150 nm<sup>2</sup> (width and stripe height). Spinstand testing demonstrated that heads with these CCP-GMR sensors are able to recover data with a BER of 10<sup>-4.3</sup> at 1420 kbp, indicating a possible areal density capability higher than the

conventional structure. In the future, more effort will be put on controlling the size and distribution of the conducting channel for even smaller sensors [49].

The dominant noise in modern sensors no longer arises from resistive (Johnson) noise or shot-noise (for TMR sensors) but from the thermal agitation of the sensor magnetization itself. As in the case of the recording medium, there is a minimum  $K_u V/kT$  that must be maintained by a sensor to assure sufficient SNR for the required bandwidth or data-rate. Here the equivalent of  $H_k$  in the sensor, often referred to as stiffness field, is a complicated function of intrinsic anisotropy, external bias fields, demagnetizing fields, current-induced fields, and exchange coupling. In addition, especially for CPP GMR devices where currents are higher, the spin-torque associated with the flow of spin-polarized electrons is a limiting consideration since it can cause the devices to go into an unstable oscillatory mode [50]. Thus several readback sensor technologies have also been proposed for future demand such as extraordinary magnetoresistance, spin FET, tunneling anisotropic magnetoresistance, and Coulomb blockade magnetoresistance.

Table. 4.3. Various design scenarios for BPM recording systems [51].

Dsgn #	AD (Tb/in <sup>2</sup> )	$W$ (nm)	$g$ (nm)	$d$ (nm)	$s_D$ (nm)	$D$ (nm)	$AR \cdot D$ (nm)	$H_A$ (kA/m)	$M_{s1}$ (kA/m)	$\delta_1$ (nm)	$\delta_{IL}$ (nm)	$M_{s2}$ (kA/m)	$\delta_2$ (nm)	BER <sub>w</sub> (dec)	BER <sub>1</sub> (dec)	BER (dec)
1	1	42	na	7.5	12.7	8.5	34	1716	1300	2	1	na	na	<-13.4	<-15	<-13.4
2	2	30	na	3.97	8.98	7.5	30	1572	1300	3	1	na	na	-2.1	-3.2	-2.0
3	3	29	na	3.24	7.33	6.5	26	3184	400	3	0.5	1200	1	-12.7	-9.5	-9.5
4	3	26	na	3.24	7.33	6.3	25	3137	600	1.75	0.5	600	4	-7.4	-8.2	-7.3
5	4	23	na	2.24	6.35	6	24	3279	400	2.75	0.5	1200	1	-5.5	-6.5	-5.5
6	5	20	na	1.75	5.66	5.5	22	3431	400	2.75	0.5	1200	0.75	-2.4	-5.2	-2.4
7	1	55	25	7.5	12.7	8	32	1388	700	2.5	na	na	na	<-15	<-15	<-15
8	2	32	17	3.97	8.98	7.5	30	1622	1300	2	na	na	na	-7.5	-9.5	-7.5
9	3	33	18	3.24	7.33	6.3	25	2583	400	2.75	na	1200	1	-5.6	-5.7	-5.4
10	1	21	na	7.5	25.4	16	16	1032	1300	6	1	na	na	-1.0	-11.3	-1.0
11	1	24	21	7.5	25.4	16	16	1037	1300	5	na	na	na	-4.3	<-15	-4.3

$W$  = pole width,  $g$  = the gap length for ring heads,  $D$  = dot dimension in down-track direction;  $AR$  = bit aspect ratio. Index 1 corresponds to the storage layer and index 2 to the soft layer in case of composite media. Common for all media  $\sigma_{sD}/s_D = \sigma_D/D = \sigma_{1A}/H_A = 0.05\%$ .

In a recording system, it is important to write sharp transitions in the medium and retain the data reliably for at least 10 years. Various design schemes for BPM at areal density 1-5 Tb/in<sup>2</sup> with its corresponding bit error rate (BER) have been proposed as can be seen in Table 4.3.

### 4.3.2. Disk Drive Electronics

Signal processing/synchronization is also an important issue to tackle in BPM technology. While the head defines all the bit locations in continuous media, the bit locations are predefined on BPM. Therefore, the head field needs to be synchronized to bit locations. Thus, any imperfections in the media fabrication process such as misplaced islands can cause write or read back errors. This will consequently require precise control on all the media property distributions such as bit size, bit location, and magnetic anisotropy [20]. The problem in signal processing/synchronization is more challenging since it is still in the research stage.

Today's disk drives use feedback (closed loop) control, as well as some other supplemental techniques. Standard feedback block diagram can be seen in Fig. 4.12. Disk drive electronics have evolved towards a minimal and economical design. A typical drive has three key integrated circuits (ICs) [50].

1. Preamplifier/write-driver mounted on the actuator.

The preamplifier sets the bias to the read head and must be able to sense and amplify the tiny readback voltages without adding much additional noise. The write-driver provides an adjustable write current plus one or two additional degrees of freedom to shape the leading edge of the transitions in the waveform. In addition to the pre-amplifier and write-driver, there is now also a 'heater driver' to provide power into the thermal actuator on each slider and thus allows the flying height to be accurately adjusted. This is an important feature to protect the delicate read and write elements from electrical overstress and electrostatic damage.

2. Motor driver or 'combo chip' that looks after both the spindle motor and the voice-coil motor (VCM) and also contains DC-DC converters.
3. Large SoC or 'system-on-chip' containing the hard-disk controller, the read/write (R/W) channel, and the high-speed interface to the outside world.

The R/W channel itself has undergone a rapid evolution starting with very simple 'peak-detect' circuits and single burst-error correcting 'Fire' codes. The error-correction schemes quickly evolved to utilize Reed-Solomon codes universally.

Modern HDDs typically use codes based on 10-bit symbols to correct 20 or more error-symbols.

In HDD, multiple controller designs, with the same structure, are optimized for different tasks, i.e. seeking, settling (transition from seeking to following), and track following.

For HDD track following:

- Reference input is the desired head position
- Measured output is the measured head position
- Error is the position error signal (PES)
- Mechanical plant consists of the driver, VCM, arm dynamics, etc.
- Disturbance consists of flutter, external vibrations, etc.

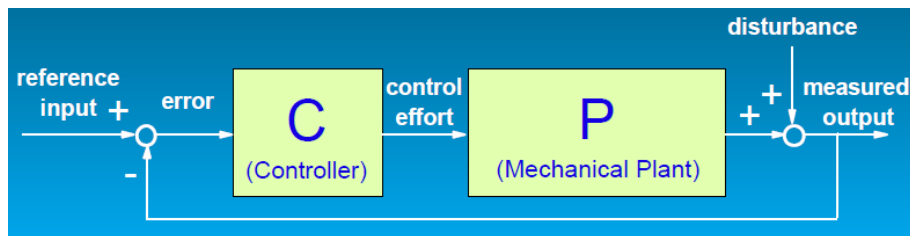


Fig. 4.12 Standard feedback block diagram [52].

Currently, data-rate has approached 2 Gb/s on the outside radius of a 15,000 rpm server drive. This poses a considerable challenge for the coupling between the read and write heads and the preamplifier and write-driver. The analog-to-digital converter in the R/W channel and much of the subsequent digital signal processing must also operate at this high clock-rate. Simple scaling to a system with an areal density of 10 Tb/in<sup>2</sup> would apparently involve data-rates exceeding 10 Gb/s. While the electronics could meet this challenge, the magnetic components themselves will struggle to reach much beyond 3 Gb/s due to gyromagnetic effects (magnetization resulting from rotation) [50].

#### 4.4. Intellectual Property

Intellectual property (IP), mainly patent, must be carefully considered before the commercialization of BPM technology. Patent grants a monopoly for the inventor of a

certain technology in a certain period of time. According to United States Patent and Trademark Office (USPTO) and Intellectual Property Office of Singapore (IPOS), a patent is generally valid for 20 years after the filing date [53],[54]. Any patents which can prevent the commercialization of BPM technology should be identified. For the following analysis, patents associated with different parts of our technology, i.e. the fabrication of the template and the media, will be discussed.

BPM technology is firstly proposed by Nakatani et al. in Japan Patent No. 888363 in 1989 [55]. Table 4.4 shows the most relevant patents to our proposed technology. It can be seen that the most relevant patents to our technology are owned by large companies in HDD industry, such as Hitachi, Toshiba, and Seagate. Thus, collaboration with large companies must be done if we want to start a company in this field.

Table 4.4. Several relevant patents to BPM.

<b>Patent # (Filing Year)</b>	<b>Ref</b>	<b>Subject</b>	<b>Assignee</b>	<b>Patent Office</b>
US 7460321 (2007)	[56]	E-beam mastering of one small arcuate portion of the master, and then replicating that portion around a circular path on the master several times to create a full disk master.	Hitachi Global Storage Tech.	USPTO
US 7471484 (2004)	[57]	A patterned medium comprised of land areas that store data and trough areas that inhibit storage of data, a write element which writes the data and a read element which reads the data and servo information.	WD Media, Inc.	USPTO
US 7306743 (2006)	[58]	A recording medium includes a substrate, and a recording layer formed on the substrate having a recording track band, and recording	Kabushiki Kaisha Toshiba	USPTO

		cells regularly arrayed in the recording track band to form a plurality rows of sub-tracks.		
US 7378028 (2004)	[59]	A method of fabricating a patterned magnetic layer which consists of forming a layer of a mask material, forming a topographical pattern, selectively removing portions of the layer of non-magnetic material, treating the exposed portions of the layer of magnetic material with a liquid for reducing the magnetic properties.	Seagate Technology LLC	USPTO
US 7347953 (2006)	[60]	Methods for forming improved self-assembled patterns of block copolymers.	IBM Corp.	USPTO
US 6,746,825 (2001)	[61]	Guided self-assembly of block copolymer films on interferometrically nanopatterned substrates.	Wisconsin Alumni Research Foundation	USPTO
US 6,926,953 (2004)	[62]	Guided self-assembly of block copolymer films on interferometrically nanopatterned substrates.	Wisconsin Alumni Research Foundation	USPTO
137768 (2007)	[63]	Data storage device with bit patterned media with staggered islands.	Seagate Technology LLC	IPOS
128567 (2006)	[64]	A method for manufacturing a patterned media in which a magnetic layer is processed in patterns of servo signals and tracks or data bits.	Kabushiki Kaisha Toshiba	IPOS



There are still rooms for us to file patents in this field. However, in manufacturing BPM, we will need assistance from patent lawyers to file patents or acquire licenses. We should also conduct further studies about how to optimize the fabrication of BPM such as:

1. Optimizing the BCP parameters such as the polymer length and Flory-Huggins parameters as well as the possibility of using other copolymers.
2. Minimizing defects in deposition of the magnetic materials process
3. Evaluating the optimum method to get planar surface and solving the overcoat process problems.

It should also be noted that if we would like to apply for a new patent, we should apply in disk-manufacturing countries, such as US, Singapore, and Malaysia.

#### 4.5. Target World Market

According to Veeco Instrument Inc., HDD industry is now in consumer era, when HDD application is not only limited to servers, desktop PC or laptop PC, but also including mobile phones, iPod, personal video recorder, and MP3, as can be seen in Fig. 4.13. These application demands enable healthy growth of HDD industry.

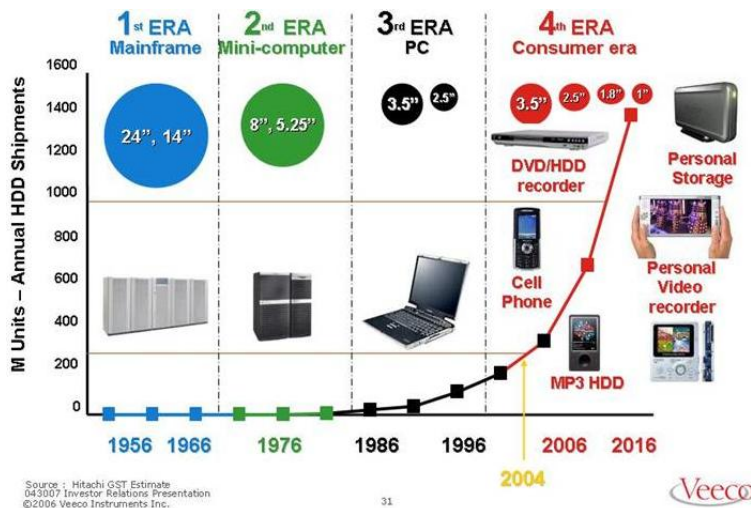


Fig. 4.13. Trend in HDD application [65].

Veeco research in 2007 provided the overall annual sales of HDDs. There has been a steady increase in the HDD sales, which is predicted to continue up to \$730 million in

2010 as can be seen in Fig. 4.14. Fig. 4.15 shows that the market is shared by several companies such as Seagate, Western Digital and Hitachi.

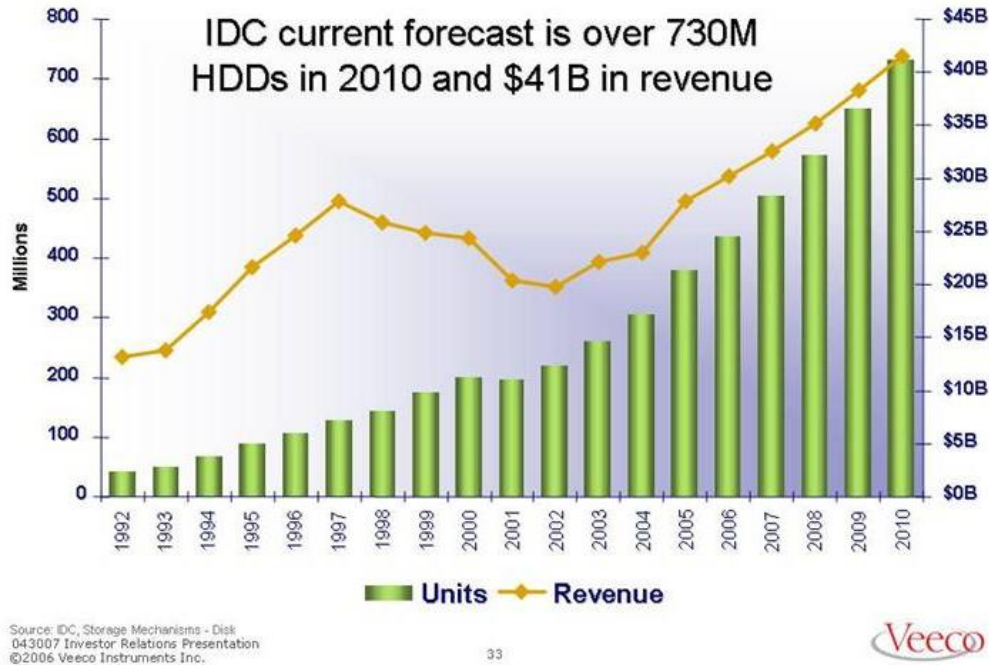


Fig. 4.14. HDD shipments and revenue [65].

Rank	Company name	Shipments (million)	Market share (%)
#1	Seagate Technology LLC (US)	175	34
#2	Western Digital Corp (US)	113	22
#3	Hitachi Global Storage (Japan)	89	17.3

(Source: iSuppli Corp, 2007)

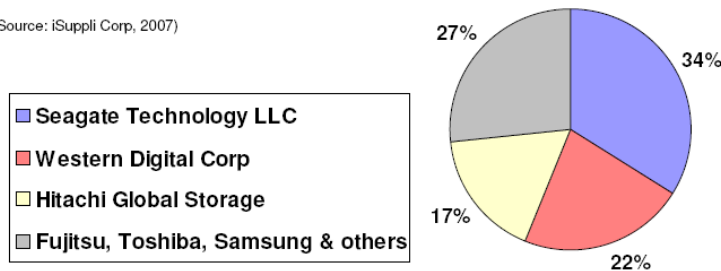


Fig. 4.15. HDD industry forecast and market share [66].

BPM, providing high areal density, will be incorporated only in high end applications, i.e. PC. The worldwide PC shipment also grows steadily as shown in Fig. 4.16. It is predicted

that the total value of worldwide PC shipments will reach 333.7 M units in 2010. BPM is likely to enter the market in 2011. If we further extrapolate this forecast, in 2011, it can be expected that the worldwide PC shipments will reach 400 M units.

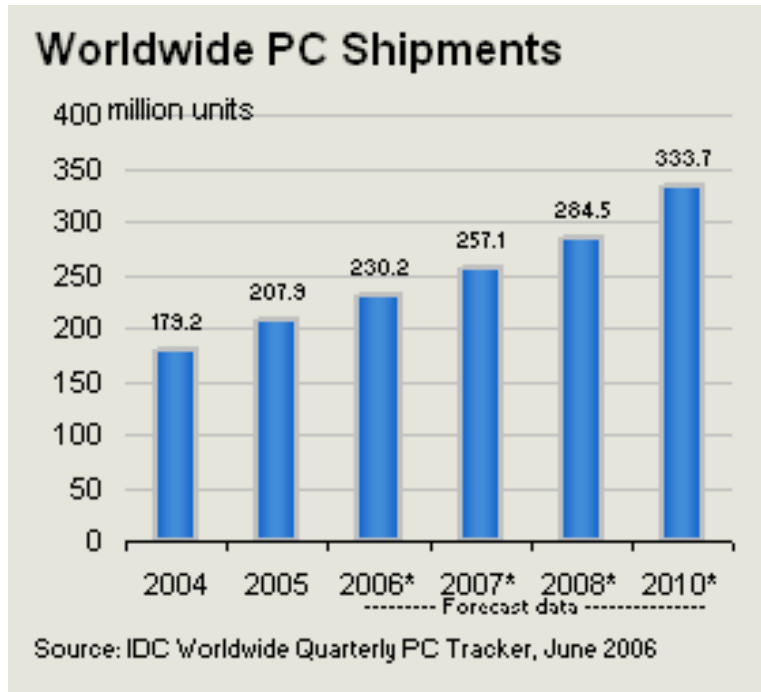


Fig. 4.16. Worldwide PC shipments forecast.

## 5. Business Plan

### 5.1. Operational Plan

One set of fundamental issues that must be addressed in a business plan is how the business will create its products. Questions that must be answered include [67]:

- What is the general approach to manufacturing? What are the sources of raw materials?
- Which processes will be used in manufacturing? What are the labor requirements?
- How will suppliers and vendors be used?

Because the business plan has the objectives of both forward planning and immediate capital raising from the investors, it is often difficult to adjust proper balance between sophistication and simplicity in explaining the sometimes complicated manufacturing and process technologies. This section will be more of a virtual operational plan, so that several simplifying assumptions will be made on the cost modeling.

There are several start-up company formats. The company may choose to, i) license the technology, ii) form a partnership, or iii) manufacture the product. Table 5.1 compares important aspects of each start up format.

Table 5.1. Comparison of start-up company formats [68].

<b>Path</b>	<b>Overhead/Organizational Complexity</b>	<b>Degree of Control</b>	<b>Funding Requirements</b>	<b>Risk</b>
<b>License</b>	Minimum	Minimum	Minimum	Minimum
<b>Alliance</b>	Moderate	Moderate	Moderate	Moderate
<b>Production</b>	Maximum	Maximum	Maximum	Maximum

Licensing a technology eliminates the need of machines, land, labor, and marketing. However, the revenue obtained is much smaller than the other two options. In strategic partnership, several companies can share responsibilities for a product. Meanwhile, in

manufacturing, high revenue can be obtained but a huge amount of funding and a complex organization are needed.

It is essential to understand how the company will manufacture its products. One way to convey such information is to examine this activity in terms of resources, processes, and output. Resources may be characterized as those elements the firm must utilize in an effort to manufacture a desired product. These typically include manufacturing facilities, machinery, equipment, materials and related assets, and labor. After describing the production resources, it is important to discuss the production processes that will be used. Finally, there should be some description of the manufacturing output. By examining the plant capacity, we may predict the potential financial performance.

Since BPM is a new fabrication method, there can be several differences from the conventional method in terms of processing techniques, which imply that there are also differences in the manufacturing tools and materials being used. As explained in Chapter 3, BPM introduces new steps into the existing media fabrication process. Therefore, what we calculate is the imposed additional cost due to the additional processing steps. The additional cost breakdown is listed in Table 5.2. Several assumptions have been made on the cost modeling:

- 1) All basic costs, such as labor, land, and materials are constant across the time period.
- 2) The cost modeling is for a 2.5” disk.
- 3) NIL output is 1 M disks/year (Appendix 2), which sets the production volume each year. NIL is actually a slow process for recording media application, as compared to the existing media fabrication scheme [27].
- 4) For pattern transfer process, we will first deposit the film and then milling it to define the islands. 1 NIL tool requires 1 ion miller to pattern the magnetic recording layer (Appendix 3).
- 5) For planarization step, every 56 NIL tools require 1 sputtering machine while every 7 NIL tools require 1 dry etcher (Appendix 4)
- 6) 1 NIL consumes 10 kW of electricity.
- 7) 1 ion miller consumes 2500 W of electricity because each cell in the miller needs 500

W (Appendix 3).

- 8) 1 sputtering machine consumes 12 kW of electricity.
- 9) 1 plasma etcher consumes 10 kW of electricity.
- 10) Cleanroom is designed for Class 10 (ISO 4) and ballroom arrangement. Economic lifetime of a cleanroom is estimated to be 15 years, equivalent to 6.67% depreciation cost per year [69].
- 11) Each tool occupies a space of 100 ft<sup>2</sup> in the clean room.
- 12) 1 master template created by EBL can create 10,000 replicas, which correspond to 100 M disks.
- 13) Labor salary is set at \$2,000/month/pax or \$24,000/year/pax.
- 14) Each machine will operate on two shifts per day, each shift is attended by two workers.
- 15) One disk consumes 1 ml of resist.
- 16) Cost for polymers (~few dollars) and silica (~hundreds of dollars) are negligible compared to other contributing factors.
- 17) Depreciation cost for the tools is 10% per year, or equivalent to 10 years of lifetime
- 18) Production volume is 100 M disks/year

Table 5.2. Additional cost breakdown for PV = 100 M disks/year and Capacity = 600 GB/disk.

ANNUAL ADDITIONAL OPERATIONAL COST BREAKDOWN FOR:					
PRODUCTION VOLUME = 100M disks/year					
AREAL DENSITY = 1 Tb/in <sup>2</sup> = 600 GB/disk					
No	Cost Component	Qty	Unit	Unit Cost/yr(\$)	Cost (\$)
1	NIL [70]	100	-	100000	10000000
2	Ion miller [71]	100	-	50000	5000000
3	Sputtering machine [72]	2	-	100000	200000
4	Plasma etcher [73]	15	-	50000	750000
5	Clean room [74]	21,700	ft <sup>2</sup>	66.67	1446739
5	EBL [75]	1	Master	480000	480000
6	Electricity [76]	8202240	kWh	0.15	1230336
7	Labor	868	-	24000	20832000
8	Resist [77]	100000	lt	200	20000000
Total Additional Cost					<b>59939075</b>
Cost/GB (cents)					<b>1.266565125</b>
Cost increase/disk (cent)					<b>59.939075</b>

## 5.2. Capitalization

Capitalization is one of the most critical parts of establishing a business. While it is sufficiently difficult to properly run a business even when sufficient resources are available, a scarcity of resources will render such an endeavor significantly more difficult. The entrepreneur has a wide variety of options to offer his or her capital providers for their participation, such as equity, debt, or hybrids such as convertible debt (debt that can be converted into equity). Rules of thumb in capital raising: [67]

- (1) Rule one is that sources and uses of capital must be equal in amount.
- (2) Rule two is not to negotiate in the business plan.

When approaching a potential source of financing, there are several guidelines: [67]

- (1) Get an introduction, if possible, from the lawyer, accountant, consultant, banker, or someone from the advisory board.
- (2) Be selective. Rather than mass mailing of business plans, it is more advisable to selectively approach attractive sources of capital and focus attention on each.
- (3) Be prepared to rethink a plan. If the entrepreneur receives consistently negative responses to a business plan, it may suggest a problem with the plan rather than a consequence of not approaching enough or the right sources.

Table 5.3. Start-up capital calculation for PV=100M disks/year.

<b>Start-up Capital Calculation</b>					
No	Cost Component	Qty	Unit	Cost (\$)	Total Cost (\$)
1	NIL [70]	100	-	1M	100,000,000
2	Ion miller [71]	100	-	0.5M	50,000,000
3	Sputtering machine [72]	2	-	1M	2,000,000
4	Plasma etcher [73]	15	-	0.5M	7,500,000
5	Clean room [74]	21,700	ft <sup>2</sup>	1000	21,700,000
5	EBL [75]	1	Master	480000	480,000
6	Electricity [76]	8202240	kWh	0.15	1,230,336
7	Labor	868	-	24000	20,832,000
8	Resist [77]	100000	lt	200	20,000,000
<b>Total Start-up Capital</b>					<b>223,742,336</b>

Raising capital can be a stressful, time-consuming activity. It often represents the first

serious obstacle to the entrepreneur. For example, a \$40B HDD industry will spend approximately \$4B annually in capital equipment [70]. Table 5.3 suggests that the start-up capital can reach ~\$200M just for the additional components to fabricate BPM. If we take into account the basic cost components to fabricate PMR, the capital needed will be much higher. It is probably not viable to expect as much funding from investors. Besides, we also need to avoid conflicts with relevant patents. Thus, only established companies such as Hitachi, Toshiba, or Seagate can implement the manufacturing of BPM. This implies that the most viable route for us, among the options in Table 5.1, is to establish a company focusing on technology licensing.

### **5.3. Financial Plan**

The purpose of the financial section of a business plan is to formulate a credible, comprehensive set of projections reflecting the company's anticipated financial performance [67]. In this section, we try to calculate the profit projection of a BPM-manufacturing company. Currently, the HDD industry is a twenty-billion-dollar market that shipped approximately 500 million units in 2007 [78]. Particularly for PC application, the market size will reach ~400 M units in 2011, as explained in Chapter 4. Regarding the vast market size, it is essential to create a well-planned financial projection as to how the BPM sales and profit of the company grows over time. In this case, we target at 25% market share, which is equivalent to production volume of 100M disks/year.

Currently, HDD price/GB is still the lowest among other type of recording media. However, provided a constant annual reduction line of 50%, SSD NAND Flash memory will reach price per GB as low as 15 cents/GB, as can be seen in Fig. 5.1. It is to common knowledge that HDD manufacturers keep reducing the price/GB, while the areal density of PMR is supposed to be locked at 500 Gb/in<sup>2</sup>, by reducing their profit margin so as to be able to compete with flash memory. Therefore, BPM has come at the right time to break the areal density limit of HDD and thus scaling down price/GB while maintaining a reasonable profit margin. It should be emphasized that Fig. 5.1 presents the price/GB of HDD products which includes cost for various processes, such as head and PCB



fabrications. Meanwhile, our calculation will focus on the media fabrication.

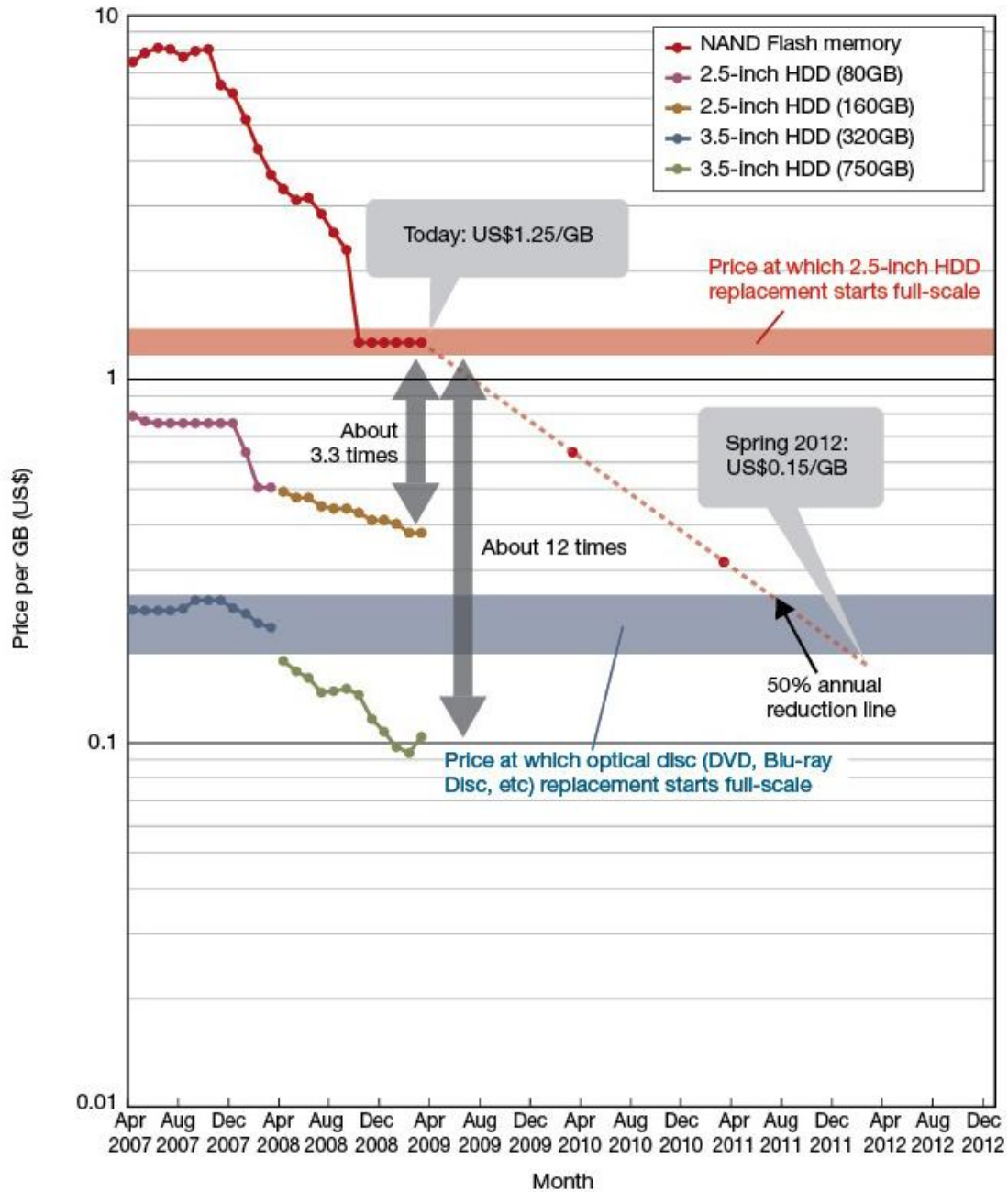


Fig. 5.1. Diagram plots of the price-per-GB for NAND Flash memory and HDDs. As of Mar 2009, NAND Flash memory is about US\$1.25 per GB. Prices through Mar 2009 from *Nihon Keizei Shimbun*, beyond that forecasts by *Nikkei Electronics* [79].

It is undeniable that SSD offers faster data rate as compared to HDD. Therefore, two major companies, Intel and Hitachi, have agreed to co-develop the new generation of SSD technology. However, SSD will complement, instead of replace, HDD. The two major companies argued that SSD will be particularly useful in storage applications that

require extremely high IOPS (Input/Output Operations per Second) [80]. Therefore, HDD will retain a secured market share in the future.

To date, HDD has been fabricated on PMR platform, which gives the current cost of HDD media at \$7/disk [27], or approximately 2 cents/GB, with an areal density limit of 500 Gb/in<sup>2</sup>, as shown in Fig. 1.1. What we calculate is the cost benefit of utilizing BPM scheme as compared to the cost of conventional PMR. BPM introduces an extra cost for utilizing NIL, ion milling, and planarization tools. However, with an areal density multiplication of two, the cost density is decreased to be approximately 1.27 cent/GB, as shown in Table 5.4.

The cost/GB can be further reduced by pushing the limit of e-beam lithography. Referring to Appendix 5, the e-beam cost will increase linearly with the areal density. However, this increase is relatively small as compared to the obtained cost benefit, as can be seen in Table 5.4. The 0.5 Tb/in<sup>2</sup> is produced by conventional PMR technology, while the 1Tb/in<sup>2</sup> and 2Tb/in<sup>2</sup> disks are produced by BPM technology.

Table 5.4. Cost modeling for 100M disk/year throughput.

<b>Areal Density (Tb/in<sup>2</sup>)</b>	<b>0.5</b>	<b>1</b>	<b>2</b>
<b>Capacity (GB/disk)</b>	300	600	1200
<b>Throughput (million disk/year)</b>	100	100	100
<b>Throughput (GB/year)</b>	30 B	60 B	120 B
<b>Reference cost</b>	\$ 700,000,000	\$ 700,000,000	\$ 700,000,000
<b>Additional cost</b>	-	\$ 59,939,075	\$ 60,419,075
<b>Total cost</b>	\$ 700,000,000	\$ 759,939,075	\$ 760,419,075
<b>Cost/GB</b>	2.33 cent	1.27 cents	0.63 cents
<b>Reduced cost/GB</b>	0	1.06 cents	1.7 cents
<b>Total cost benefit</b>	0	\$ 636 M	\$ 2,040 M
<b>Cost increase/disk</b>	0	59.94 cent	60.42 cent

For other production volume, we plot the cost/GB as shown in Fig. 5.2. It can be seen that as we increase the production volume, the cost/GB will drop in an exponential manner. Fig. 5.3 depicts cost/GB as a function of both production volume and areal density of the HDD. It can be seen that either increasing the areal density or the production volume will reduce the cost/GB.

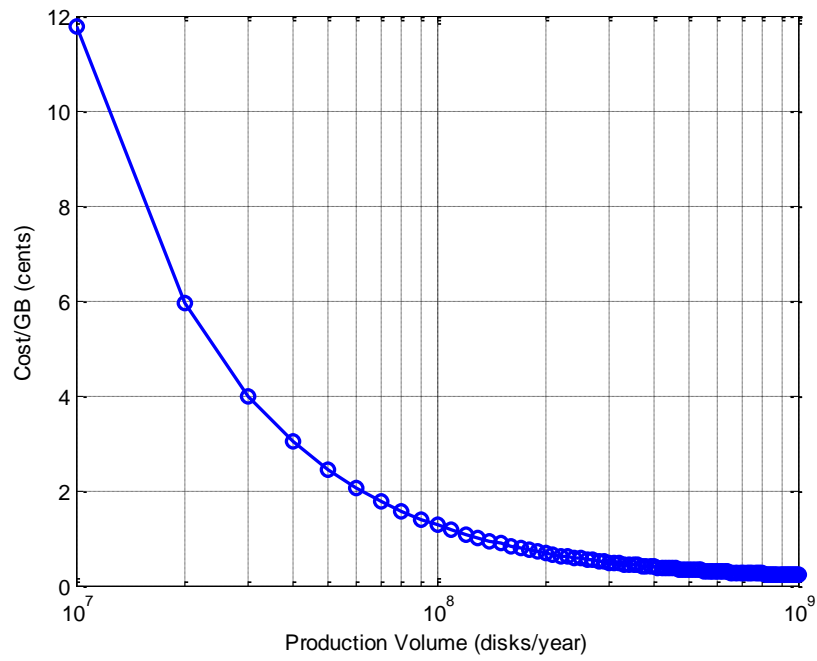


Fig. 5.2. Cost/GB for 1Tb/in<sup>2</sup> as a function of production volume.

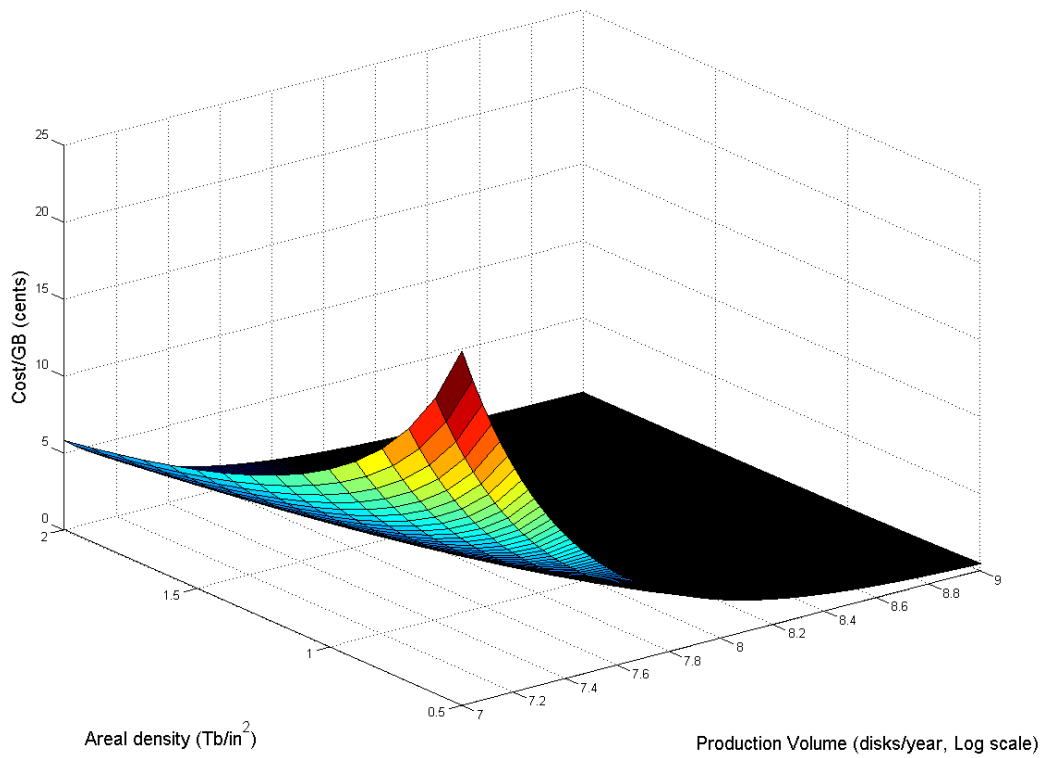


Fig. 5.3. Cost/GB as a function of production volume and areal density.

The calculation of cost benefit assumes that the consumer would want to purchase the improved HDD capacity with constant price/GB. This assumption, unfortunately, is not plausible. In fact, for an increase of areal density from 0.5 to 1 Tb/in<sup>2</sup>, the increase of cost per disk should be less than \$1 [27]. This is equivalent to say that the increase of cost per disk should not exceed ~15% for a doubling of areal density.

The question now is that for a given areal density (or HDD capacity), how low should the cost per GB be in order to be acceptable in the market. Let  $C_{disk}$ ,  $AD$ ,  $C$ ,  $C_p$  be the cost per disk, areal density, cost per GB and HDD capacity, respectively. Then,

$$\begin{aligned}
C_{disk,max} &= 1.15^{\log_2\left(\frac{AD}{AD_0}\right)} C_{disk,0} \\
&= 2^{\log_2 1.15 \times \log_2\left(\frac{AD}{0.5}\right)} \times \$7 = 7 \times 2^{\log_2\left(\frac{AD}{AD_0}\right)^{\log_2 1.15}} \\
&= 7 \times \left(\frac{AD}{0.5}\right)^{0.2016} = 8.0498(AD)^{0.2016} \\
C_{max} \times C_p &= 7 \times \left(\frac{AD}{0.5}\right)^{0.2016} \\
C_{max} &= \frac{7}{AD \frac{Tb}{in^2} \times \left(\frac{1}{4} \pi \times 2.5^2 in^2\right) \times \frac{1000Gb}{1Tb} \times \frac{1GB}{8Gb}} \times \left(\frac{AD}{0.5}\right)^{0.2016} \\
&= \frac{7}{613.59 AD} \times \left(\frac{AD}{0.5}\right)^{0.2016} = \frac{1.1408 \times 10^{-2}}{AD} \times \left(\frac{AD}{0.5}\right)^{0.2016} = \frac{0.01312}{AD^{0.7984}}
\end{aligned}$$

$C_{disk,max}$  and  $C_{max}$  are plotted as a function of areal density in Fig. 5.4. Based on the information from Fig. 5.4, we can now re-draw Fig. 5.3 in contour representation, as shown in Fig. 5.5, to determine our profit margin. For example, for 1 Tb/in<sup>2</sup>, market will only accept a maximum cost/GB of ~1.33. Therefore, the contour plot sets a minimum production volume of approximately 80M disks/year (10<sup>7.9</sup> disks/year) as the break-even point. Thus, our chosen production volume of 100M disks/year in this cost modeling is reasonable.

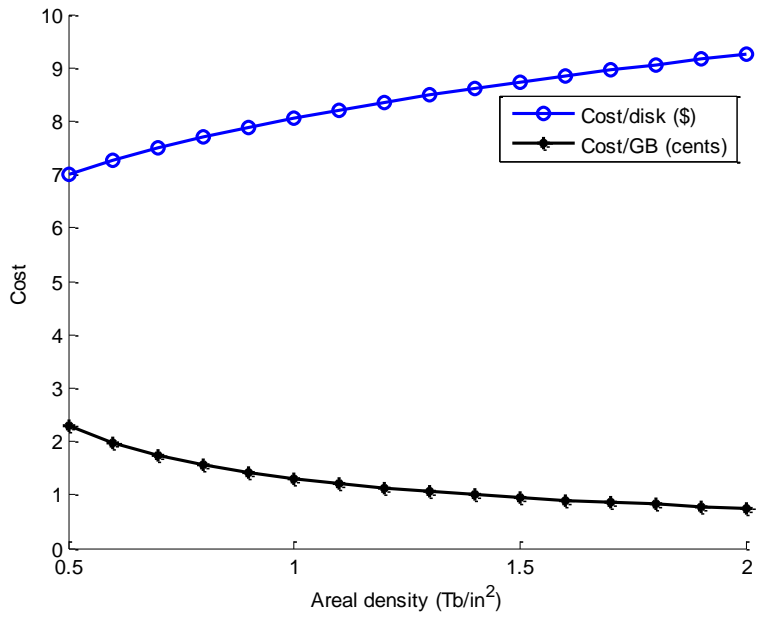


Fig. 5.4. Maximum cost per disk and cost per GB for different areal densities.

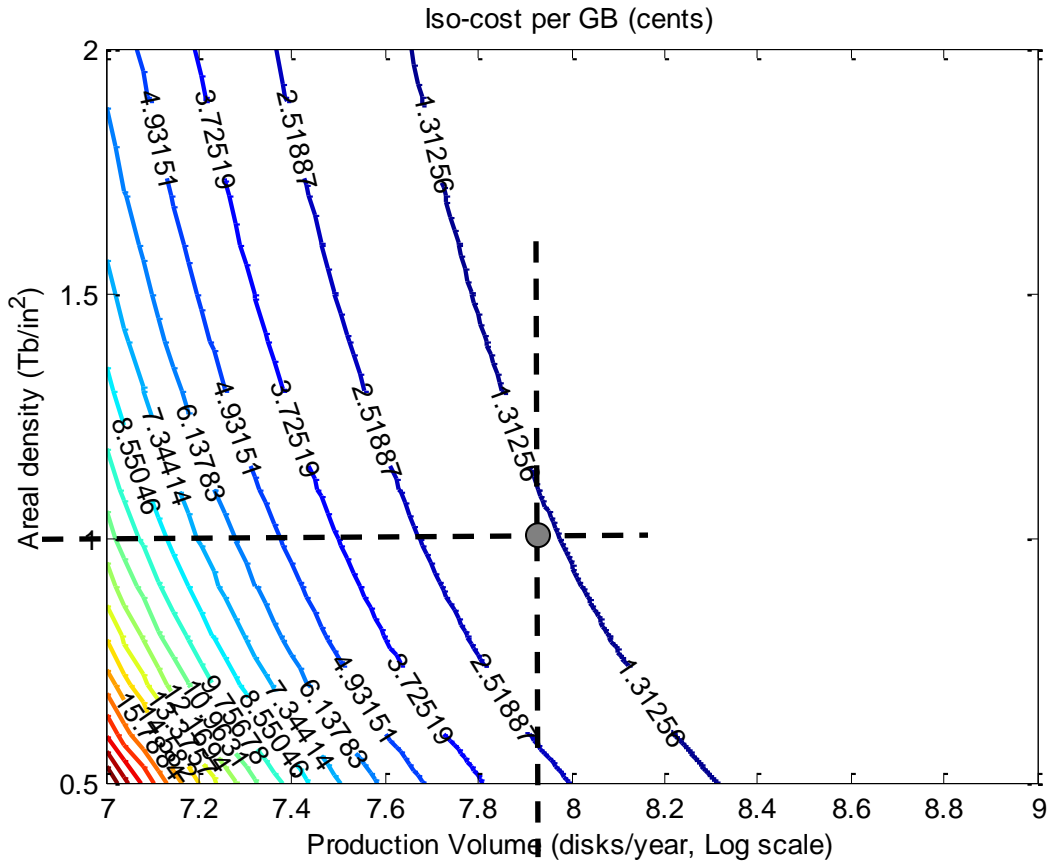


Fig. 5.5. Contour representation of cost/GB as a function of production volume and areal density

We can then define profit as,

$$\begin{aligned} \text{Profit} &= (\text{Cost}/\text{GB}_{\max} - \text{Cost}/\text{GB}) \times \text{Production volume} \times \text{HDD Capacity} \\ &= (C_{\max} - C) \times PV \times C_p \end{aligned}$$

where  $C_p = 613.59 \times AD$ , assuming 2.5" disk. Since  $C_{\max}$  decreases over time,  $C$  should decrease in a faster rate to ensure a profitable company. This will be the case if BPM technology can consistently increase the areal density. BCP has a characteristic length scale that can ideally be tuned to be very small, in the order of sub-10 nm [81]. BCP resolution of 12.7 nm (1 Tb/in<sup>2</sup>) has been demonstrated in 2008 [28],[82]. Currently, the best achievable resolution of BCP is 3 nm [19]. Meanwhile, e-beam lithography has a resolution that is limited by the beam spot size. With various aberrations present in the system (spherical, chromatic, and diffraction), state-of-the-art resolution of e-beam system is ~10 nm [83]. Head technology will be ready for 1 Tb/in<sup>2</sup> areal density in 2011, as shown in Fig. 4.9 (a). This fact is consistent if we assume an annual rate of 50% for the projection in Fig. 1.1.

Mathematically, we can write,

$$AD(x) = 1.5^{x-2011} \frac{Tb}{in^2}$$

Along this line, it is projected that the areal density will reach 5 Tb/in<sup>2</sup> in 2015, equivalent to BCP resolution of 5.7 nm, which is obviously achievable. Therefore, the areal density increase in overall will be limited by the head capability to read and write the tiny features in BPM.

Table 5.4 suggests that the incremental additional cost for an areal density increase is attributed to the EBL cost. So, the total cost can be expressed as,

$$\begin{aligned} \text{Total cost} &= \text{Reference cost} + \text{Additional cost} \\ &= \$700\text{M} + \left( \$59,459,075 + \frac{AD}{1Tb/in^2} \times \$480,000 \right) \\ &= \$759,459,075 + \frac{AD}{1Tb/in^2} \times \$480,000 \end{aligned}$$

Thus, the profit can be written as,

$$\begin{aligned}
 \text{Profit}(x) &= (C_{\max} - C) \times PV \times C_p \\
 &= C_{\max} \times PV \times C_p - \text{Total cost} \\
 &= \left( \frac{0.01312}{AD(x)^{0.7984}} \right) \times (10^8) \times (613.59 \times AD(x)) - \left( 7.5946 \times 10^8 + \frac{AD(x)}{1Tb/in^2} \times 480000 \right) \\
 &= 8.0503 \times 10^8 AD(x)^{0.2016} - 480000 AD(x) - 7.5946 \times 10^8 \\
 &= 8.0503 \times 10^8 (1.5^{x-2011})^{0.2016} - 480000 (1.5^{x-2011}) - 7.5946 \times 10^8
 \end{aligned}$$

It is also important to define a profit margin,

$$\text{Profit margin}(x) = \frac{\text{Profit}(x)}{\text{Revenue}(x)} \times 100\%$$

which can be calculated as follow,

$$\begin{aligned}
 \text{Profit margin}(x) &= \frac{8.0503 \times 10^8 (1.5^{x-2011})^{0.2016} - 480000 (1.5^{x-2011}) - 7.5946 \times 10^8}{8.0503 \times 10^8 (1.5^{x-2011})^{0.2016}} \times 100\% \\
 &= \left( 1 - 5.9625 \times 10^{-4} (1.5^{x-2011})^{0.7984} - 0.9434 (1.5^{x-2011})^{-0.2016} \right) \times 100\%
 \end{aligned}$$

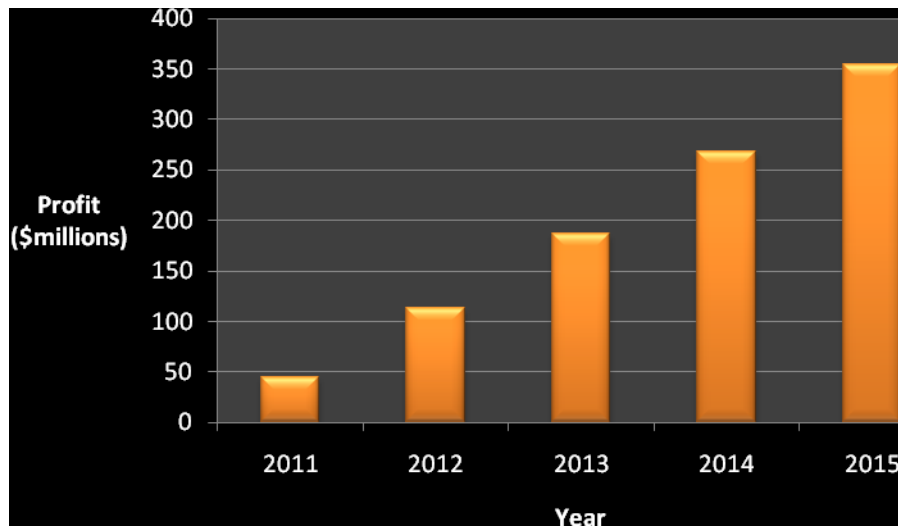


Fig. 5.6. Annual profit projection of HDD media company with BPM technology.

The annual profit projection is given in Fig. 5.6. As can be seen, the profit increases steadily with time starting from ~\$50 M in 2011 up to ~\$350 M in 2015. Since the required start-up capital is approximately \$200M, this means that the company will reach

the break-even point in the third operational year. The profit margin also increases from ~5% up to more than 30% in five-year operational time, as shown in Fig. 5.7. The actual timeframe for BCP technology is however hard to predict, considering its potential to reach a very high areal density if combined with other technologies.

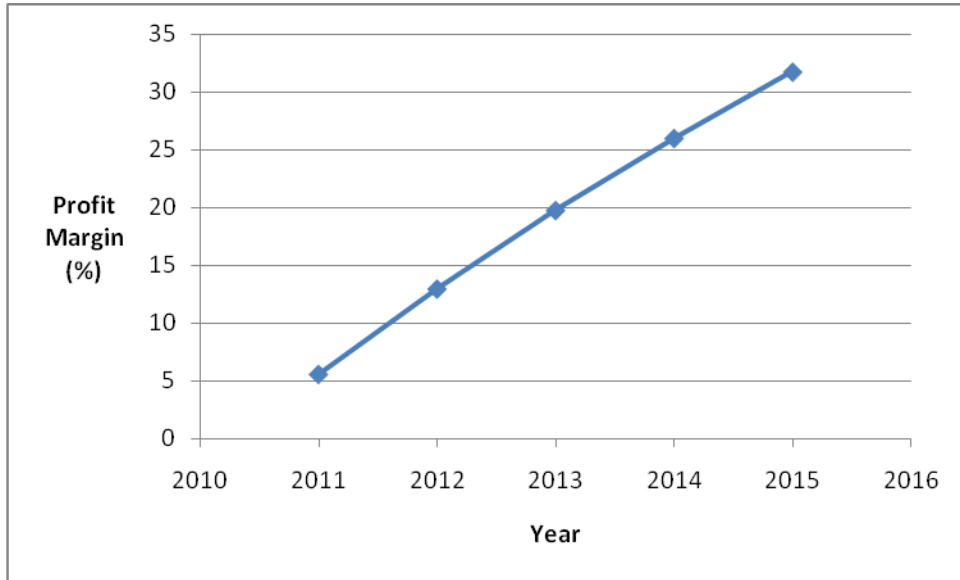


Fig. 5.7. Profit margin projection of HDD media company with BPM technology.



## 6. Conclusion

BPM is a way to surpass the areal density limit in current HDD media, without compromising the SNR and writability. BPM technology has overcome major technological barrier even though it still needs further research to become a mature technology. Hitachi and Seagate have set a common fabrication platform for BPM which combines both top-down and bottom-up approaches. Combination of EBL and chemically-assisted self-assembly process of BCP to fabricate the master template provides areal density beyond 1 Tb/in<sup>2</sup>, while the use of UV-NIL for template replication and disk production ensure the required high throughput. The fabrication plan inserts some new steps into the traditional PMR disk process flow, meaning that the existing PMR fabrication tools are still compatible for BPM industry in the future.

In HDD supply chain, BPM technology will play a role in the media fabrication. The competing technologies, such as HAMR and ECC, may come out first. However, BPM can be integrated in HAMR and ECC to enhance their performance, thus showing their mutual synergy. Areal density must increase while low cost must be maintained in order for HDD to keep dominating the market over its closest competitor, solid-state memory. Head and disk drive electronics as the complementary technologies are also developing fast. It is predicted that CPP GMR will be able to read 1Tb/in<sup>2</sup> data in 2011, setting the scene for BPM to enter the market. Prior to that, DTM technology will govern. There are still many improvements to pursue in BPM technology. Thus, it is possible to apply for patents as we do more intensive research. We should file patents in countries where HDD media are made, such as US, Singapore, and Malaysia.

It has been shown that our fabrication method is superior in terms of performance and cost compared to the conventional media. As calculated in the business plan, the future of BPM industry is bright, with steadily increasing annual profit, as the areal density increases. The market share of BPM is very large with the worldwide PC shipments is predicted to reach 400 M units in 2011. In this consumer era, BPM will survive in the market as long as they can meet the consumer demand of high areal density. According to the business plan for 5-year period, the profit increases steadily with time starting from

~\$50 M in 2011 up to ~\$350 M in 2015, with profit margin increases from ~5% to 30%. The actual timeframe for BCP is difficult to estimate. BPM areal density is predicted to be able to reach 10 Tb/in<sup>2</sup>. However, if combined with other technologies such as HAMR, it can potentially reach 100Tb/in<sup>2</sup>. To fabricate BPM, we need to consider the patent conflicts as well as the huge amount of capital. Thus, only established companies might pursue the manufacturing of BPM.

## References

- [1] "www.eetasia.com."
- [2] M. Camras, *Magnetic Recording Handbook*, Springer, 1988.
- [3] S.X. Wang and A.M. Taratorin, *Magnetic Information Storage Technology*, Academic Press, 1999.
- [4] R. New, "The Future of Magnetic Recording Technology," Apr. 2008.
- [5] R. Sbiaa and S.N. Piramanayagam, "Patterned Media Towards Nano-bit Magnetic Recording: Fabrication and Challenges," *Recent Patents on Nanotechnology*, vol. 1, 2007, p. 29.
- [6] A. Kikitsu, Y. Kamata, M. Sakurai, and K. Naito, "Recent progress of patterned media," *IEEE Transactions on Magnetics*, vol. 43, 2007, pp. 3685-3688.
- [7] C.A. Ross, "Magnetic Recording: Patterned Media," *Encyclopedia of Materials: Science and Technology*, Elsevier Science Ltd., 2001, pp. 4912-4919.
- [8] X. Yang, S. Xiao, K. Lee, D. Kuo, and D. Weller, "From nano-imprint lithography to self-assembly-pattern generation for bit patterned media beyond 1Tbit/in<sup>2</sup>," 53rd Annual Conference on Magnetism and Magnetic Materials, Texas: 2008.
- [9] D. Kercher, "Manufacturing strategies for discrete track and bit-patterned media," 53rd Annual Conference on Magnetism and Magnetic Materials, Texas: 2008.
- [10] "<http://www.ndt-ed.org/EducationResources/CommunityCollege/MagParticle/Physics/HysteresisLoop.htm>."
- [11] J.C. Mallinson, *The Foundations of Magnetic Recording, Second Edition*, Academic Press, 1993.
- [12] C. Kittel, "Physical Theory of Ferromagnetic Domains," *Rev. Mod. Phys.*, vol. 21, 1949, pp. 541-583.
- [13] N.A. Spaldin, *Magnetic Materials: Fundamentals and Device Applications*, Cambridge University Press, 2003.
- [14] J.S. Miller and M. Drillon, *Magnetism: Molecules to Materials III Nanosized Magnetic Materials*, Wiley VCH, 2001.
- [15] K.M. Rabe, *Physics of Ferroelectrics: A Modern Perspective*, Springer, 2007.
- [16] "[http://lmis1.epfl.ch/webdav/site/lmis1/shared/Files/Lectures/Nanotechnology%20for%20engineers/Archives/2004\\_05/Superparamagnetism.pdf](http://lmis1.epfl.ch/webdav/site/lmis1/shared/Files/Lectures/Nanotechnology%20for%20engineers/Archives/2004_05/Superparamagnetism.pdf)."
- [17] J.C. Lodder, "Methods for preparing patterned media for high-density recording," *Journal of Magnetism and Magnetic Materials*, vol. 272, 2004, pp. 1692-1697.
- [18] "Hard Disk Drives from Hitachi Global Storage Technologies," <http://www.hitachigst.com/portal/site/en/menuitem.368c8bfe833dee8056fb11f0aac4f0a0/>.
- [19] S. Park, D.H. Lee, J. Xu, B. Kim, S.W. Hong, U. Jeong, T. Xu, and T.P. Russell, "Macroscopic 10-Terabit-per-Square-Inch Arrays from Block Copolymers with Lateral Order," *Science*, vol. 323, 2009, pp. 1030-1033.
- [20] B.D. Terris, "Fabrication challenges for patterned recording media," *Journal of Magnetism and Magnetic Materials*, vol. 321, 2009, pp. 512-517.
- [21] B.D. Terris, T. Thomson, and G. Hu, "Patterned media for future magnetic data storage," *Microsystem technologies*, vol. 13, 2007, pp. 189-196.
- [22] G.M. Schmid, M. Miller, C. Brooks, N. Khusnatdinov, D. LaBrake, D.J. Resnick,

- S.V. Sreenivasan, G. Gauzner, K. Lee, and D. Kuo, "Step and flash imprint lithography for manufacturing patterned media," *Journal of Vacuum Science & Technology B: Microelectronics and Nanometer Structures*, vol. 27, 2009, p. 573.
- [23] Y. Kamata, A. Kikitsu, H. Hieda, M. Sakurai, K. Naito, J. Bai, and S. Ishio, "Microscopic Magnetic Characteristics of CoCrPt-Patterned Media Made by Artificially Aligned Self-Organized Mask," *Japanese Journal of Applied Physics*, vol. 46, 2007, pp. 999-1002.
- [24] A. Kikitsu, "Prospects for bit patterned media for high-density magnetic recording," *Journal of Magnetism and Magnetic Materials*, vol. 321, 2009, pp. 526-530.
- [25] C.A. Ross, "Patterned magnetic recording media," *Annual Review of Materials Research*, vol. 31, 2001, pp. 203-235.
- [26] S.N. Piramanayagam, "Perpendicular recording media for hard disk drives," *Journal of Applied Physics*, vol. 102, Jul. 2007, pp. 011301-22.
- [27] S. N. Piramanayagam, "EE5202 Lecture Notes," 2009.
- [28] R. Ruiz, H. Kang, F.A. Detcheverry, E. Dobisz, D.S. Kercher, T.R. Albrecht, J.J. de Pablo, and P.F. Nealey, "Density multiplication and improved lithography by directed block copolymer assembly," *Science*, vol. 321, 2008, p. 936.
- [29] J. Cheng, C. Ross, H. Smith, and E. Thomas, "Templated Self-Assembly of Block Copolymers: Top-Down Helps Bottom-Up," *Advanced Materials*, vol. 18, 2006, pp. 2505-2521.
- [30] T. Miyazaki, K. Hayashi, K. Kobayashi, Y. Kuba, H. Ohyi, T. Obara, O. Mizuta, N. Murayama, N. Tanaka, Y. Kawamura, and H. Uemoto, "Potential of a rotary stage electron beam mastering system for fabricating patterned magnetic media," *Journal of Vacuum Science Technology B: Microelectronics and Nanometer Structures*, vol. 26, 2008, p. 2611.
- [31] S. Ouk Kim, H.H. Solak, M.P. Stoykovich, N.J. Ferrier, J.J. de Pablo, and P.F. Nealey, "Epitaxial self-assembly of block copolymers on lithographically defined nanopatterned substrates," *Nature*, vol. 424, Jul. 2003, pp. 411-414.
- [32] M. Park, C. Harrison, P.M. Chaikin, R.A. Register, and D.H. Adamson, "Block Copolymer Lithography: Periodic Arrays of  $\sim 10^{11}$  Holes in  $1\mu\text{m}^2$  Square Centimeter," *Science*, vol. 276, May. 1997, pp. 1401-1404.
- [33] D. Yamaguchi, S. Shiratake, and T. Hashimoto, "Ordered Structure in Blends of Block Copolymers. 5. Blends of Lamella-Forming Block Copolymers Showing both Microphase Separation Involving Unique Morphological Transitions and Macrophase Separation<sup>†</sup>," *Macromolecules*, vol. 33, Oct. 2000, pp. 8258-8268.
- [34] K. Asakawa, T. Hiraoka, H. Hieda, M. Sakurai, Y. Kamata, and K. Naito, "Nano-Patterning for Patterned Media using Block-Copolymer," *Journal of Photopolymer Science and Technology*, vol. 15, 2002, pp. 465-470.
- [35] I. Bitá, J.K.W. Yang, Y.S. Jung, C.A. Ross, E.L. Thomas, and K.K. Berggren, "Graphoepitaxy of Self-Assembled Block Copolymers on Two-Dimensional Periodic Patterned Templates," *Science*, vol. 321, Aug. 2008, pp. 939-943.
- [36] P. Hofemann, "Hard disk drive industry driving areal density and lithography," Sep. 2008.
- [37] P. Gourevitch, R. Bohn, and D. McKendrick, "Globalization of production: Insights from the hard disk drive industry," *World development*, vol. 28, 2000, pp. 301-317.
- [38] R. de Souza and H.P. Khong, "Supply chain models in hard disk drive

- manufacturing,” *IEEE Transactions on Magnetics*, vol. 35, Mar. 1999.
- [39] H.J. Richter, “Density limits imposed by the microstructure of magnetic recording media,” *Journal of Magnetism and Magnetic Materials*, vol. 321, 2009, pp. 467-476.
- [40] M. Koji, I. Akihiro, and H. Shin-Ya, “Thermally Assisted Magnetic Recording,” *Fujitsu Sci Tech J*, vol. 42, 2006, pp. 158-167.
- [41] “Seagate Technology,” [www.seagate.com](http://www.seagate.com).
- [42] O. Heinonen and K.Z. Gao, “Extensions of perpendicular recording,” *Journal of Magnetism and Magnetic Materials*, vol. 320, 2008, pp. 2885–2888.
- [43] R.E. Rottmayer, S. Batra, D. Buechel, W.A. Challener, J. Hohlfeld, Y. Kubota, L. Li, B. Lu, C. Mihalcea, K. Mountfield, and others, “Heat-assisted magnetic recording,” *IEEE Transactions on Magnetics*, vol. 42, 2006, pp. 2417–2421.
- [44] J. Zhu, X. Zhu, and Y. Tang, “Microwave Assisted Magnetic Recording,” *IEEE Transactions on Magnetics*, vol. 44, Jan. 2008, pp. 125-131.
- [45] C. Thirion, W. Wernsdorfer, and D. Mailly, “Switching of magnetization by nonlinear resonance studied in single nanoparticles,” *Nature materials*, vol. 2, 2003, pp. 524–527.
- [46] Jian-Ping Wang, Weikang Shen, and J. Bai, “Exchange coupled composite media for perpendicular magnetic recording,” *Magnetics, IEEE Transactions on*, vol. 41, 2005, pp. 3181-3186.
- [47] M.H. Kryder, E.C. Gage, T.W. McDaniel, W.A. Challener, R.E. Rottmayer, G. Ju, Y.T. Hsia, and M.F. Erden, “Heat assisted magnetic recording,” *Proceedings of the IEEE*, vol. 96, 2008, pp. 1810-1835.
- [48] K. Nagasaka, “CPP-GMR technology for magnetic read heads of future high-density recording systems,” *Journal of Magnetism and Magnetic Materials*, vol. 321, Mar. 2009, pp. 508-511.
- [49] X. Peng, P. Kolbo, K. Nikolaev, S. Chen, Z. Wang, T. Boonstra, P. Anderson, S. Kalderon, P. Czoschke, A. Morrone, D. Dimtrov, S. Xue, and Y. Chen, “Current-confined-path (CCP) giant magnetoresistive (GMR) sensors,” *Journal of Magnetism and Magnetic Materials*, vol. 321, Jun. 2009, pp. 1889-1892.
- [50] R. Wood, “Future hard disk drive systems,” *Journal of Magnetism and Magnetic Materials*, vol. 321, 2009, pp. 555–561.
- [51] H. Richter, A. Dobin, O. Heinonen, K. Gao, R. Veerdonk, R. Lynch, J. Xue, D. Weller, P. Asselin, M. Erden, and R. Brockie, “Recording on Bit-Patterned Media at Densities of 1 Tb/in<sup>2</sup> and Beyond,” *Magnetics, IEEE Transactions on*, vol. 42, 2006, pp. 2255-2260.
- [52] “<http://www.hitachigst.com/hdd/research/images/as%20images/servoloops.pdf>.”
- [53] “United States Patent and Trademark Office Home Page.”
- [54] “IPOS - Intellectual Property Office of Singapore.”
- [55] A. Kikitsu, Y. Kamata, M. Sakurai, and K. Naito, “Recent progress of patterned media,” *IEEE Transactions on Magnetics*, vol. 43, 2007, pp. 3685-3688.
- [56] Z.Z. Bandic and T. Wu, “United States Patent: 7460321 - System, method, and apparatus for forming a patterned media disk and related disk drive architecture for head positioning,” U.S. Patent 7460321, December 2, 2008.
- [57] D. Wachenschwanz, M. McNeil, and J. Vicars, “United States Patent: 7471484 - Patterned medium and recording head,” U.S. Patent 7471484, December 30, 2008.

- [58] H. Hieda, M. Sakurai, K. Asakawa, T. Hiraoka, and K. Naito, "United States Patent: 7306743 - Recording medium, method of manufacturing recording medium and recording apparatus," U.S. Patent 7306743, December 11, 2007.
- [59] K. Wago, H. Wang, N. Kurataka, G. Gauzner, and N. Deeman, "United States Patent: 7378028 - Method for fabricating patterned magnetic recording media," U.S. Patent 7378028, May 27, 2008.
- [60] C.T. Black, R. Rulz, and R.L. Sandstrom, "United States Patent: 7347953 - Methods for forming improved self-assembled patterns of block copolymers," U.S. Patent 7347953, March 25, 2008.
- [61] P.F. Nealey, J.J. DePablo, F. Cerrina, H.H. Solak, X. Yang, R.D. Peters, and Q. Wang, "United States Patent: 6746825 - Guided self-assembly of block copolymer films on interferometrically nanopatterned substrates," U.S. Patent 6746825, June 8, 2004.
- [62] P.F. Nealey, J.J. DePablo, F. Cerrina, H.H. Solak, X. Yang, R.D. Peters, and Q. Wang, "United States Patent: 6926953 - Guided self-assembly of block copolymer films on interferometrically nanopatterned substrates," U.S. Patent 6926953, August 9, 2005.
- [63] H. J. Richter, A.Y. Dobin, and D.K. Weller, "Data storage device with bit patterned media with staggered islands," May. 2007.
- [64] A. Kikitsu, Y. Kamata, S. Shirotori, and M. Sakurai, "Method and apparatus for manufacturing patterned media," Jun. 2006.
- [65] "Veeco Provides Enabling Technology in Process Equipment and Metrology for Multiple Growth Markets," Apr. 2007.
- [66] "<http://www.isuppli.com>."
- [67] B.R. Ford, J.M. Bornstein, P.T. Pruitt, and E.&. Young, *The Ernst & Young Business Plan Guide*, Wiley, 2007.
- [68] "MDA Technology Applications Program," <http://www.mdatechnology.net/>.
- [69] L. Yang and C. Eng Gan, "Costing small cleanrooms," *Building and Environment*, vol. 42, 2007, pp. 743–751.
- [70] D. Lammers, "MII Tackles Patterned Media Opportunity - 5/22/2008 9:26:00 AM - Semiconductor International."
- [71] "<http://www.iciequipment.com/catalog1.htm>."
- [72] "<http://www.tomcoughlin.com/Techpapers/Diskcon%202007%20LN3%20Posters,%20091207.pdf>."
- [73] W. Menz, J. Mohr, and O. Paul, *Microsystem Technology*, Wiley-VCH, 2001.
- [74] "[http://www.idc-ch2m.com/services/cleanroom/cleanroom\\_cost.asp](http://www.idc-ch2m.com/services/cleanroom/cleanroom_cost.asp)."
- [75] "<http://www.nanolithography.gatech.edu/services.html>."
- [76] "[http://en.wikipedia.org/wiki/Electricity\\_tariff](http://en.wikipedia.org/wiki/Electricity_tariff)."
- [77] "<http://www.micromagazine.com/archive/05/04/pham.html>."
- [78] "[http://www.molecularimprints.com/NewsEvents/news\\_articles07/HDDsale.pdf](http://www.molecularimprints.com/NewsEvents/news_articles07/HDDsale.pdf)."
- [79] "<http://techon.nikkeibp.co.jp/article/HONSHI/20090528/170918/fig6.jpg>."
- [80] "[http://news.cnet.com/8301-13924\\_3-10110921-64.html](http://news.cnet.com/8301-13924_3-10110921-64.html)."
- [81] S. Park, O. Park, J.Y. Cheng, C.T. Rettner, and H. Kim, "Patterning sub-10 nm line patterns from a block copolymer hybrid," *Nanotechnology*, vol. 19, 2008, p. 455304.

- [82] J.Y. Cheng, Charles T. Rettner, Daniel P. Sanders, Ho-Cheol Kim, and William D. Hinsberg, "Dense Self-Assembly on Sparse Chemical Patterns: Rectifying and Multiplying Lithographic Patterns Using Block Copolymers," *Advanced Materials*, vol. 20, 2008, pp. 3155-3158.
- [83] C. Ross, "3.47 Lecture Notes," 2009.
- [84] A. Halperin, J.U. Sommer, and M. Daoud, "Copolymers at striped surfaces: Coupling effects," *Europhysics Letters*, vol. 29, 1995, pp. 297-297.
- [85] "<http://www.molecularimprints.com/Products/I2200page.html>."
- [86] "Imprio HD2200," <http://www.molecularimprints.com/Products/I2200page.html>.
- [87] "<http://www.atomtech.co.uk/FAB104.html>."
- [88] L.S. Miller and J.B. Mullin, *Electronic materials*, Springer, 1991.
- [89] "[www.sdt.sz.com/document/SDT-2000%20Spec.doc](http://www.sdt.sz.com/document/SDT-2000%20Spec.doc)."
- [90] "CNF - Lab and Equipment Information," [http://www.cnfusers.cornell.edu/cnf5\\_tool.taf?\\_function=detail&eq\\_id=70&labUser=1&\\_UserReference=BCB6991EC0134A7F45FE911F](http://www.cnfusers.cornell.edu/cnf5_tool.taf?_function=detail&eq_id=70&labUser=1&_UserReference=BCB6991EC0134A7F45FE911F).
- [91] "JEOL JBX-9300FS Electron Beam Lithography System Training," [http://www.nanolithography.gatech.edu/JEOL\\_JBX-9300FS\\_Training.pdf](http://www.nanolithography.gatech.edu/JEOL_JBX-9300FS_Training.pdf), Jun. 2009.
- [92] H. Takemura, H. Ohki, H. Nakazawa, Y. Nakagawa, M. Isobe, Y. Ochiai, T. Ogura, M. Narihiro, and T. Mogami, "Performance of new E-beam lithography system JBX-9300FS," *Microelectronic Engineering*, vol. 53, Jun. 2000, pp. 329-332.

## Appendix 1: Block Copolymers on Chemically Heterogeneous Striped Surface [84]

Fig. A1.1 shows block copolymers adsorption on the chemically heterogeneous striped surface. Consider AB diblock copolymers on surface consisting of alternating rectangular domains  $\alpha$  and  $\beta$  of equal width  $L$ . Each of the stripes only has affinity toward one of the block species. In this case, block A and block B consist of equal number of monomers ( $N_A=N_B=N_n$ ) and the adsorption energies of an A(B) energies on an  $\alpha(\beta)$  are  $\delta$ . The copolymer is modeled as an ideal Gaussian chain.

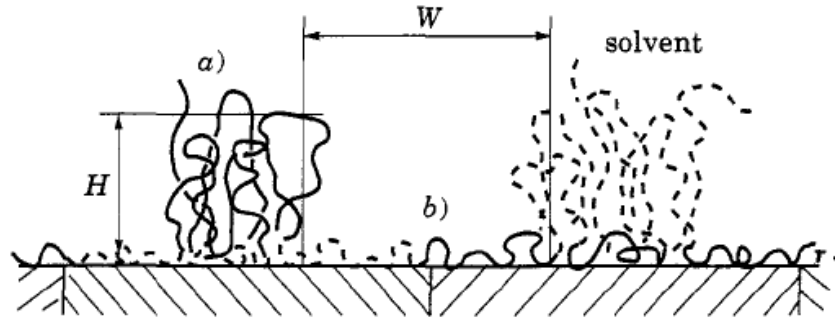


Fig. A1.1. When the width of the stripes is much larger than the size of a block, the copolymers may either form 3D brushes within each stripe (a) or 2D brushes along the interfaces between the stripes (b) [84].

We consider the case of dilute, non-interacting boundaries. As shown in Fig. A1.1, the adsorbed layer consists of two regions: (i) Central regions, coated by a polymer brush formed from the adsorption of AB diblock copolymers onto the selectively adsorbing surface. (ii) Narrow boundary regions near the  $\alpha\beta$  border in which the adsorbed layer has the structure of 2D planar brush.

The copolymer adsorption is analyzed by minimizing the free-energy density. Within the boundary regions, the free energy per block for two-dimensional brush is:

$$F/kT \approx -N_n \delta^{5/3} + N_n \Gamma^2 \delta + \Gamma W^2 / N_n a^2 \quad \dots \text{(A.1-1)}$$

with,

$$\Gamma \approx N_n a^2 / \lambda W \quad \dots \text{(A.1-2)}$$

where  $\Gamma$  is the monomer area fraction,  $a$  is the monomer size, and  $\lambda$  is the length of the



boundary segment of A and B junction. The first two terms correspond to the adsorption free energy ( $F_{ads}$ ) and the interaction free energy ( $F_{int}$ ) in the two-dimensional semi-dilute layer respectively. Meanwhile, the third term takes into account the Gaussian elastic penalty of the stretched string ( $F_{el}$ ).

The linear free-energy density is:

$$\tau = (F_A + F_B)/\lambda = 2F/\lambda \quad \dots \text{(A.1-3)}$$

$$\frac{\tau}{kT} = \frac{F}{kT} \frac{2}{\lambda} = -\frac{2N_n \delta^{5/3}}{\lambda} + \frac{2N_n^3 a^4 \delta}{\lambda^3 W^2} + \frac{2W}{\lambda^2} \quad \dots \text{(A.1-4)}$$

We need to satisfy two conditions:

$$\frac{\partial \tau}{\partial W} = 0 \quad \dots \text{(A.1-5)}$$

$$\text{and } \frac{\partial \tau}{\partial \lambda} = 0 \quad \dots \text{(A.1-6)}$$

For a fixed  $\lambda$ ,  $W$  can be determined as follow:

$$\begin{aligned} \frac{\partial \tau}{\partial W} &= 0 \\ -\frac{4N_n^3 a^4 \delta}{\lambda^3 W^3} + \frac{2}{\lambda^2} &= 0 \\ W^3 &= \frac{2N_n^3 a^4 \delta}{\lambda} \\ W &\approx N_n \left( \frac{a}{\lambda} \right)^{1/3} \delta^{1/3} a \quad \dots \text{(A.1-7)} \end{aligned}$$

The equilibrium state corresponds to:

$$F_{int} \approx F_{el} = \frac{W}{\lambda} \approx N_n \left( \frac{a}{\lambda} \right)^{4/3} \delta^{1/3} \quad \dots \text{(A.1-8)}$$

Thus the linear free-energy density becomes:

$$\frac{\tau}{kT} \approx -\frac{N_n \delta^{5/3}}{\lambda} + N_n \left( \frac{a}{\lambda} \right)^{4/3} \frac{1}{\lambda} \delta^{1/3}$$

$$\frac{\tau a}{kT} \approx -N_n \delta^{5/3} \left(\frac{a}{\lambda}\right) + N_n \left(\frac{a}{\lambda}\right)^{7/3} \delta^{1/3} \quad \dots \text{(A.1-9)}$$

Put the result back to equation (A.1-6):

$$\frac{\partial \tau}{\partial \lambda} = 0$$

$$N_n \delta^{5/3} \frac{a}{\lambda^2} - \frac{7}{3} N_n \frac{a^{7/3}}{\lambda^{10/3}} \delta^{1/3} = 0$$

$$\delta^{4/3} = \frac{7}{3} \frac{a^{4/3}}{\lambda^{4/3}}$$

Thus, we get:

$$\lambda \approx \left(\frac{a}{\delta}\right) \quad \dots \text{(A.1-10)}$$

Combining (A.1-10) with (A.1-7), we get:

$$W \approx N_n \delta^{2/3} a$$

The central region ceases to exist, i.e. the boundary regions cover the whole of the surface, when:

$$L = L^* = 2W \approx 2N_n \delta^{2/3} a$$

The width of the stripes must also be larger than the adsorption blob size  $D$  for the adsorption blobs to be defined. Thus, for A and B blocks to be registered on  $\alpha$  and  $\beta$  surfaces while maintaining close packing of adsorption,  $L$  must satisfy  $D < L < L^*$ .

## Appendix 2: NIL Cost Calculation



Fig A2.1. Imprio<sup>®</sup> HD2200 [85].

The specification of the tool [86]:

- Resolution: Sub-20 nm, half-pitch for discrete track and bit patterned media
- Throughput (double-sided): 180 disks per hour
- Alignment: <10 microns (relative to disk spindle hole)
- Disk Automation: Fully automated cassette-to-cassette and template loading

We assume working time of ~16 hrs/day. Then,

$$\text{Throughput} = 180 \frac{\text{disks}}{\text{hour}} \times 16 \frac{\text{hours}}{\text{day}} \times 360 \frac{\text{days}}{\text{year}} \approx 1M \frac{\text{disks}}{\text{year}}$$

$$\text{NIL cost} = \frac{\text{Production Volume}}{\text{Throughput}} \times \text{NIL cost/unit}$$

For PV = 100 M disks/year,

$$\text{NIL cost} = \frac{100M \frac{\text{disks}}{\text{year}}}{1M \frac{\text{disks}}{\text{year}}} \times \$1M = \$100M$$

### Appendix 3: Ion Miller Throughput Calculation



Fig. A3.1. FAB104 ion miller system [87].

#### Specifications:

- Capacity: 5 cells
- Max. equivalent current output (mA/cell): 10
- Beam energy range (KeV): 0.65-2.1
- Max. power input (W/cell): 500
- Max. plasma current (mA/cell): 200
- Applied high voltage range (kV): 1-2.5
- Typical Ar gas flow (sccm/cell): 15
- Typical operating pressure (mbar):  $1 \times 10^{-3}$
- Pumping speed requirement (L/sec/cell): 500
- Min. cooling water (L/min@20°C): 2

Typical etch rate for ion milling system is 1-2  $\mu\text{m/hr}$ . [88]

Each magnetic layer has a thickness of 15 nm, thus

$$t_{5 \text{ disks}} = \frac{15 \text{ nm}}{1 \frac{\mu\text{m}}{\text{hr}}} = 0.015 \text{ hr}$$

$$t_{180 \text{ disks}} = \frac{180}{5} \times 0.015 = 0.54 \text{ hr} \approx 1 \text{ hr}$$

Thus, NIL and ion miller have the same throughput rate.

## Appendix 4: Sputtering and Dry Etching Machine Throughput Calculation

Sputtering machine specification (SDT-2000):[89]

- Substrate: Disc (material: poly-carbonate) of 120 mm in diameter and 1.2 mm in thickness
- Output : 1.8 sec/disc (~70 nm film thickness)
- Exhaust system: Turbo molecular pump: 210 liters/sec  
Oil rotary pump: 360 liters/min
- Sputtering source: P-GUN 170CD type (Target Outer Ring of herisert)
- Power supply: DC 12kW

$$t_{1\text{ disk}} = \frac{15\text{nm}}{75\text{nm} / 1.8\text{sec}} = 0.36\text{sec}$$

$$\text{Throughput} = \frac{1\text{disk}}{0.36\text{sec}} = 2.8\text{disks} / \text{sec} = 10000\text{disks} / \text{hr}$$

So, approximately 56 NIL tools require only one sputtering machine.



Fig. A4.1. PT770 Dry Etcher system [90].

Specification:

- Ambient:  $\text{Cl}_2$ ,  $\text{BCl}_3$ ,  $\text{H}_2$
- Etch rate (A/min): 3000
- Selectivity: 10:1 oxide, 0.7:1 resist
- Substrate size: 3 inch, 100 mm

Assuming that each disk should be etched ~15 nm deep (comparable to the magnetic layer thickness), the throughput of the etcher is

$$t_{1 \text{ disk}} = \frac{15nm}{300nm / \text{min}} = 0.05 \text{ min}$$

$$\text{Throughput} = \frac{1 \text{ disk}}{0.05 \text{ min}} = 20 \text{ disks / min} = 1200 \text{ disks / hr}$$

Approximately 7 NIL tools require only one dry etcher machine. Thus, the overall throughput is limited by NIL (180 disks/hr).

## Appendix 5: EBL Cost Calculation



Fig. A5.1. JBX-9300FS EBL system [91].

### Specifications:

- 4nm diameter Gaussian spot electron beam
- 50kV/100kV accelerating voltage
- 50pA – 100nA current range
- 50MHz scan speed, however maximum scan speed has been demonstrated to be 25MHz [92]
- +/- 100um vertical range automatic focus
- +/- 2mm vertical range manual focus
- ZrO/W thermal field emission source
- vector scan for beam deflection
- max 300mm (12") wafers with 9" of writing area
- < 20nm line width writing at 100kV
- < 20nm field stitching accuracy at 100kV
- < 25nm overlay accuracy at 100kV

### Assumptions:

- Wafer size,  $d_{wafer} = 2.5''$  or  $r_{wafer} = 3.175$  cm
- Digital field ( $B$ ) = 14 bits
- Settling time ( $t_{settle}$ ) = 4 sec

BPM allows a spatial frequency multiplication of two, or an areal density multiplication

of four, from the pattern as-defined by EBL. However, the actual features (pixel size) to be written are in the size of the BCP domains. Assuming that one pixel is assigned for one magnetic island and one magnetic island has the dimension of half the period, we can calculate the required pixel size for 1 Tb/in<sup>2</sup> as follow,

$$A_{bit} = \frac{1}{\text{Areal density}} = \frac{1}{1 \frac{Tb}{in^2}} = 10^{-12} in^2$$

$$d_{bit} = \sqrt{10^{-12} in^2} = 25.4nm$$

$$d_{pixel} = \frac{1}{2} d_{bit} = 12.7nm$$

In fact, the required pixel size can even be smaller due to the requirement of 5% accuracy for the feature locations. The field size ( $A_{field}$ ) is then,

$$A_{field} = 2^{2B} (A_{pixel}) = 2^{28} (12.7nm)^2 = 43295.95 \mu m^2$$

Number of field ( $N$ ),

$$N = \frac{A_{wafer}}{A_{field}} = \frac{\pi (3.175 \times 10^4 \mu m)^2}{43295.95 \mu m^2} = 73145.90 = 73146$$

Total pattern generation time ( $T_{pg}$ ),

$$T_{pg} = N \frac{2^{2B}}{f} = 73146 \frac{2^{28}}{(25 \times 10^6 Hz)} = 7.854 \times 10^5 sec = 218.17hrs$$

Total settling time,

$$T_{settle} = N \times t_{settle} = 73146 \times 4 = 292584 sec = 81.27hrs$$

Total time ( $t$ ),

$$t = T_{pg} + T_{settle} = 218.17 + 81.27 = 299.44 hrs \approx 300hrs \approx 13days$$

From [75], rate of EBL usage for industry is \$1600/hr,

$$\text{Cost (EBL)} = 300 \times \$1600 = \$480,000 \sim \$0.5M$$

EBL cost for any other areal density can then be calculated as,

$$\text{Cost of EBL} = \frac{\text{Areal density}}{1 \frac{Tb}{in^2}} \times \$480,000$$